Lattice Boltzmann modeling of flow field in a lid-driven cavity under slip boundary conditions

THESIS SUBMITTED IN PARTIAL FULFILMENTS OF THE REQUIREMENT FOR THE DEGREE OF MASTER OF ENGINEERING IN MECHANICAL ENGINEERING UNDER FACULTY OF ENGINEERING AND TECHNOLOGY

Submitted by

MD SULTAN

Class Roll Number: 002011202014

Exam Roll No.: M4MEC22014

Registration Number: 154313 of 2020-21

Academic Session: 2020-2022

Under the guidance of

Dr. Himadri Chattopadhyay

Professor
Department of Mechanical Engineering

Jadavpur University

DEPARTMENT OF MECHANICAL ENGINEERING

JADAVPUR UNIVERSITY

KOLKATA- 700032, INDIA

2022

DECLARATION OF ORIGINALITY AND COMPLIANCE OF ACADEMIC ETHICS

I hereby declare that the thesis entitled "**Lattice Boltzmann modelling of flow field in a lid - driven cavity under slip boundary condition**" contains literature survey and original research work by the undersigned candidate, as a part of his ***MASTER OF TECHNOLOGY IN MECHANICAL ENGINEERING*** studies during academic session 2020-2022.

All information in this document have been obtained and presented in accordance with the academic rules and ethical conduct.
I also declare that, as required by these rules of conduct, I have fully cited and referenced all the material and results that are not original to this work.

Name: **MD SULTAN**

Class Roll Number: **002011202014**

University Registration No: **154313 of 2020-21**

Thesis Title: **Lattice Boltzmann modeling of flow field in a lid-driven cavity under slip boundary conditions.**

Date:

Signature: _____

FACULTY OF ENGINEERING & TECHNOLOGY

DEPARTMENT OF MECHANICAL ENGINEERING

JADAVPUR UNIVERSITY

KOLKATA

CERTIFICATE OF RECOMMENDATION

This is to certify that the thesis entitled ‘‘**Lattice Boltzmann modelling of flow field in a lid - driven cavity under slip boundary condition**’’ is a bona fide work carried out by **Md Sultan** under our supervision and guidance in partial fulfillment of the requirements for awarding the degree of **Master of Technology in Mechanical Engineering** under Department of Mechanical Engineering, Jadavpur University during the academic session 2020-2022.

Thesis Advisor

Dr. Himadri Chattopadhyay

Professor

Department of Mechanical Engineering

Jadavpur University, Kolkata

Prof. (Dr.) Chandan Mazumdar

Dean

Faculty Council of Engineering and Technology

Jadavpur University, Kolkata

Prof. (Dr.) Amit Karmakar

Head of Department

Department of Mechanical Engineering

Jadavpur University, Kolkata

FACULTY OF ENGINEERING AND TECHNOLOGY

DEPARTMENT OF MECHANICAL ENGINEERING

JADAVPUR UNIVERSITY

KOLKATA

CERTIFICATE OF APPROVAL

The foregoing thesis entitled "**Lattice Boltzmann modelling of flow field in a lid -driven cavity under slip boundary condition**" is hereby approved as a creditable study of Mechanical Engineering and presented in a satisfactory manner to warrant its acceptance as a pre-requisite to the degree of "**Master of Mechanical Engineering"** at the department of Mechanical Engineering, Jadavpur University, Kolkata700032, for which it has been submitted. It is understood that by this approval the undersigned do not necessarily endorse or approve any statement made, opinion expressed or conclusion drawn therein but approve the thesis only for the purpose for which it is submitted.

Committee on Final Examination
For Evaluation of the Thesis

Signature of Examiners

ABSTRACT

Flow in lid driven cavity is a very well-known problem due to its complex flow structure and involvement of associated physics. The lid-driven cavity problem is commonly encountered in various MEMS-based applications such as lubrication technologies, micro-pumps, micro-heat exchangers, electronic-cooling, food processing, nuclear reactors etc. Incorporation of Slip boundary conditions in a lid driven cavity flow is a very attractive research area because it captures the non-equilibrium (or) rarefaction effects near the walls and removes the singularity presents in the corner of the cavity where moving and stationary walls intersect.

LBM is a new method for simulating fluid flow problem. LBM has shown great potentials for solving complex fluid systems. LBM is based on mesoscopic kinetic particles and can incorporate interparticle interaction directly. Due to its kinetic nature LBM has found to be an effective tool for numerical simulation involving interfacial dynamics.

Flow field in a lid driven square cavity with slip boundary conditions are investigated in this work using LBM. While the range of Re is varied, between 20 to 300, slip boundary conditions are implemented for a tangential momentum accommodation coefficient (σ) up to 0.01. Simulations has been carried out using SRT- LBM. To account for the slip, two different methods are used for boundary conditions, namely tangential momentum accommodation coefficient (TMAC) and modified bounce-back specular reflection (MBSR). It is observed that the MBSR scheme generates extra numerical slip compared to TMAC scheme. Results show that appearance of secondary vortex is affected by the slip coefficient. While for Re = 50, as the slip coefficient reduces, secondary vortex develops at $\sigma = 0.1$, for Re =100, the threshold slip coefficient is 0.05. With reducing value of σ i.e., as the effect of slip increases, the location of the vortex centre shifts towards the centre of the cavity.

ACKNOWLEDGEMENTS

I would like to express my grandest gratitude to Prof. Himadri Chattopadhyay, Department of Mechanical Engineering, Jadavpur University for his excellent and resourceful guidance, which helped me a lot in the completion of my thesis. Without his supervision and constant encouragement, it would not be possible to prepare such a thesis compactly. I do covey my best regards and gratitude to him.

I would like to thank to the respected teachers in mechanical engineering department of Jadavpur University for their valuable suggestions and cooperation from time to time.

I would like to separately thank Runa Samanta, PhD Research Scholar, Department of Mechanical Engineering, Jadavpur University, without whose initiative and support it would not have been possible to carry out this project.

I would like to express my gratitude towards my parents and my family members for their kind cooperation and encouragement which helped me in completion of my master's thesis.

Contents

List of Tables and Figures

List of Figure Captions

List of Tables

Nomenclature

c_i	discrete lattice velocity in direction i (m/s)
c_f	skin friction co-efficient
c_s	sound speed of the model (m/s)
f_i	density distribution function in direction i (kg/m^3)
f_i^{eq}	equilibrium distribution function in direction i (kg/m^3)
H	length and height of the domain
Kn	Knudsen number
l_s	slip length
Re	Reynolds number, $\frac{Hu_o}{\nu}$
u	x-component velocity
v	y-component velocity
u_o	lid velocity (m/s)
x, y	cartesian coordinates (m)

Greek symbols

Δt	time step (s)
Δx	lattice space (m)
λ	mean free path
μ	dynamic viscosity (kg/m-s)
ν	kinematic viscosity (m^2/s)
ρ	density (kg/m^3)
σ	Tangential momentum accommodation coefficient

τ relaxation time

w_i weight coefficient in direction i

Subscripts

i direction i in a lattice

o reference variable

w wall

Chapter 1

OVERVIEW

1.1 Introduction

According to continuum approach in fluid dynamics, fluid molecules in the immediate vicinity of a solid wall move at the same speed of the wall. However, the scenario in microscopic level is different in which fluids exhibit a net fluid motion relative to the solid wall, known as slip motion. And the slip motion is measured by the slip length (l_s) which is defined as the linearly extrapolated distance from the wall where the fluid speed matches exactly the wall speed. Slip length is proportional to mean free path (λ) of molecules.

Traditional numerical simulations based on continuum approach and the Navier-Stokes equations break down at higher values of the Knudsen number (Kn), which is the ratio of the mean free path of the gas molecules λ to the characteristic length H of the flow domain. According to Knudsen number range, the state of a gaseous flow can be defined in four different regimes. First, the gaseous flow for Kn < 0.001 is known as continuum regime and the Navier-Stokes equations with classical no-slip boundary conditions are accurately applicable in this regime. Next, the gaseous flow range for Knudsen number 0.001 < Kn < 0.1 is known as slip flow regime where a velocity slip and a temperature jump are taken into account at the wall and 0.1< Kn <10 is termed as transition regime and in this regime the continuum approach of the Navier-Stokes equation is no longer valid. For Kn > 10 the regime can be considered as free molecular flow regime.

The study of fluid flows in microdevices specially in MEMS has received much more attention in recent years because the fluid flow behavior deviates significantly from the traditional no-

slip flow. Rarefied gas flows with slip boundary conditions are often countered in the micro-scale devices. The lid-driven cavity problem is commonly encountered in various MEMS-based applications such as lubrication technologies, micro-pumps, micro-heat exchangers, electronic-cooling, food processing, nuclear reactors etc. [**1-3**]. Slip is often encountered in screw-extruders **[4**] which are used for food and polymer processing. The transport phenomena in a screw-extruder can be closely approximated as a lid-driven cavity flow as shown in an LBM simulation by Buick and Cosgrove [**5**]. Many researchers used Particle based methods such as Molecular Dynamics (MD) and the Direct Simulation Monte Carlo (DSMC) methods to simulate such microflows. But computation time in LBM is significantly less compared to DSMC. Execution time for the LBM with single relaxation time is in the order of minute, while the solving time for the DSMC method is in the order of day.

Flow in lid driven cavity is a very well-known problem due to its complex flow structure and involvement of associated physics. Many researchers have been investigated lid driven cavity flow with different geometries, boundary conditions as well as lid movement configurations [**6-9**]. Besides lid driven cavity flow analyzed by various computational methods like the Navier-Stokes-Fourier equations (NSF) **[10**], Direct Simulation Monte Carlo (DSMC) [**11**],[**12**] method and moment equations approach [**13**].

Incorporation of Slip boundary conditions in a lid driven cavity flow is a very attractive research area because it captures the non-equilibrium (or) rarefaction effects near the walls and removes the singularity presents in the corner of the cavity where moving and stationary walls intersect. Mizzi et al. [**14**] presented the solutions of a micro lid-driven square cavity using Navier-Stokes-Fourier equations and compared them with their DSMC results for the Boltzmann equation. Importantly, they found that while the Navier-Stokes-Fourier model could predict the velocity field well outside of kinetic boundary layers, it could not compute

accurate solutions to other aspects of flow in the slip regime. Darbandi et al. [**15**] simulated micro lid-driven cavity flow with various aspect ratios using finite volume element method. Rana et al. [**16**] analyzed the lid-driven cavity using a finite difference scheme to compute steady state solutions of the regularized 13 moment (R13) equations of rarefied gas dynamics.

The lattice Boltzmann method (LBM) has been proved an alternative powerful numerical tool for simulating fluid flows on complex micro-geometries since it can recover the Navier–Stokes equations with Chapman-Enskog-expansions. In the beginning of the development, most of the researchers focused on the problems in which they applied nonslip boundary conditions. But in micro-channel experiments, it has been observed that the measured mass flow rate is higher than that based on a non-slip boundary condition [**17**]. The most popular scheme applied is the bounce-back scheme because of its easy implementation. However, the bounce-back scheme has been proved that it would generate a nonzero slip velocity [**18**].

A lot of researches have been done on various flow domain in which non-slip boundary condition is applied using LBM [**19-24**]. Sauro Succi (2002) [**25**] first introduced a mesoscopic lattice Boltzmann model with a suitable boundary condition that is the combination of bounce back and specular reflections to analyze the efficiency of catalytic micro-channel. That is basically a lattice implementation of a physical model of boundary phenomena proposed by Maxwell in 1879. On the other hand, In the last two decades there has been significant progress in the development of Micro-electro-mechanical systems (MEMS) and Nano-technology with micro-scale size, such as microchannel flows at the application and as well as at the simulation levels [**26**] using LBM. The study of gaseous flow in these micro and nano-devices has been an interesting and active topic of research in recent days because it captures the rarefaction effects. Therefore, many researches applied the LBM with various slip boundary conditions to the microscale fluid systems [**27-33**]. Many investigations were performed in the past where

various slip boundary conditions such as CBC (Combined bounce back condition), CBSR (Combined bounce back and specular reflection), DSBC (Diffused scattering and bounce back condition) & MBSR (Modified bounce back and specular reflection) etc. mostly used for rarified gas flow within micro-channel to analyze micro-Couette flow or micro-Poiseuille flow [**34-42**].

The state-of-art survey as carried out above indicates that while the flow field in lid driven cavity is extensively investigated, the same under the influence of wall slip is rather poorly studied. The importance of studying the slip flow is becoming more relevant for present day miniaturization involving microelectromechanical systems [MEMS], extruder system. Thus, the present work examines the flow structure in a lid driven cavity under slip boundary condition using two types of boundary conditions which are **TMAC (**Tangential momentum accommodation coefficient**)** [**43**] and **MBSR (**Modified bounce back and specular reflection) [**44**] scheme**.**

The paper is organized in five sections. In Section 2 problem description and mathematical modeling are discussed. In section 3 some aspects of the LBM with governing equation and associated boundary conditions are discussed. Section 4 includes the results and discussions. Finally in Section 5 concluding remarks are made.

1.2 Literature review

Elguennouni et al. (2020) **[8**] investigated a lid-driven flow inside an isosceles triangular cavity numerically. The range of Knudsen numbers discussed was from the slip to the early transition regime. To capture non-equilibrium effects near the walls, slip boundary conditions were used. According to their analysis It is clear that the SRT-LBM loses its validity with increasing the rarefaction degree while the MRT-LBM findings approximate well with those obtained by the DSMC method. In the slip regime, for small values of the Knudsen number, the results demonstrate that both methods are good alternatives, but in the transition regime, only MRT-LBM shows its capability to describe the gas microflows usually found in the MEMS devices.

Mizzi et al. (2007) [**14**] presented the solutions of a micro lid-driven square cavity using Navier-Stokes-Fourier equations and compared them with their DSMC results for the Boltzmann equation. Importantly, they found that while the Navier-Stokes-Fourier model could predict the velocity field well outside of kinetic boundary layers, it could not compute accurate solutions to other aspects of flow in the slip regime.

Rana et al. (2012) [**16**] analyzed the lid-driven cavity using a finite difference scheme to compute steady state solutions of the regularized 13 moment (R13) equations of rarefied gas dynamics.

He et al. (1997) [**18**] used the standard bounce-back rule to impose nonslip boundary conditions in macroscopic flows leads to an artificial quadratic dependence of the slip flow at the wall on the Knudsen number. They simulated the micro cavity flow and observed that at small Knudsen numbers the vortex center moves downward and the mass flow rate increases with increasing Kn. On contrast, at high Knudsen numbers the vortex center moves upward and the mass flow

rate decreases with Knudsen number, which is attributed to the fact that the slip velocity on the upper wall causes momentum transfer less efficient.

Sauro Succi (2002) [**25**] first introduced a mesoscopic lattice Boltzmann model with a suitable boundary condition that is the combination of bounce back and specular reflections. That is basically a lattice implementation of a physical model of boundary phenomena proposed by Maxwell in 1879. He investigated the slip motion as a function of the reflectivity of the solid wall by means of this mesoscopic lattice Boltzmann model. He observed the slip flow for reflectivity values below a critical threshold. From the numerical result it is shown that the slip motion significantly affects the conversion efficiency (degrades the efficiency of microreactive channels) of catalytic microchannels.

Ansumali and Karlin (2002) extended the derivation of the lattice Boltzmann method from the continuous kinetic gas theory proposed by He et al. (1997) in order to obtain accurate boundary conditions for the method. They derived the boundary condition for the discrete set of velocities for the model of a diffusively reflecting moving solid wall. Numerical results are presented which demonstrate convergence to the hydrodynamic limit. In particular, the Knudsen layer in the Kramer's problem is reproduced correctly for small Knudsen numbers.

Sbragaglia and Succi (2005) [**28**] presented a mathematical formulation of kinetic boundary conditions for lattice Boltzmann schemes in terms of reflection, slip, and accommodation coefficients. It was shown that, in the presence of a nonzero slip coefficient, the lattice Boltzmann develops a physical slip flow component at the wall which can be matched exactly to analytical and experimental data up to second order in the Knudsen term, well inside the transition regime ($0 < Kn < 0.8$). This means that the lattice Boltzmann scheme with kinetic boundary conditions can be used to predict slip flow at finite Knudsen numbers well beyond the strict hydrodynamic limit.

Sofonea and Sekerka (2005) [**29**] conducted a systematic study of the effect of various boundary conditions (bounce back and three versions of diffuse reflection) for the two-dimensional first-order upwind finite difference Lattice Boltzmann model. They simulated Couette and Poiseuille flow in a micro-channel using the diffuse reflection boundary condition and revealed the existence of a slip velocity that depends on the Knudsen number and the lattice spacing. The best results were obtained for diffuse reflection boundary conditions that allow thermal mixing at a wall located at half lattice spacing outside the boundary nodes.

Zhang et al. (2006) [**30**] proposed a wall-function approach for the effective mean free path that enables lattice Boltzmann methods to be extended beyond the slip-flow regime. For planar Couette flow, the results indicate that the method significantly improves the accuracy of lattice Boltzmann models, especially in the near-wall region, and it has been shown that the method provides a reasonable description of the nonlinear flow characteristics in the Knudsen layer up to $Kn \sim O(1)$.

Guo et al. (2006) [**31**] studied systematically the physical symmetry, spatial accuracy, and relaxation time of the lattice Boltzmann equation (LBE) for micro gas flows in both the slip and transition regimes. The model proposed in this work LBE(BRT) not only satisfies the consistency requirement but also takes into account the influence of the wall confinement. Numerical tests show that this treatment can improve the accuracy of the LBE for simulating microgas flows with a relatively large Knudsen number.

Benzi et al. (2005) [**32**] implemented a suitable boundary condition for a discrete version of the Boltzmann equations describing a wall-bounded single-phase fluid. They distinguished different slippage properties on the surface by introducing a slip function, defining the local degree of slip for hydrodynamical fields at the boundaries. They studied the mesoscopic slip properties in terms of slip length, slip velocity, pressure drop reduction (drag reduction), and

mass flow rate in microchannels as a function of the degree of slippage and of its spatial distribution and localization.

Yang et al. (2019) [**48**] investigated the Couette and Poiseuille flow in micro channel with TMAC and MBSR slip scheme and concluded that TMAC is more accurate than MBSR. They clarified the defects of the existing slip boundary conditions through theoretical analysis and improved the boundary conditions proposed by Kuo and Chen (2009) [**43**].

Mohammed and Reis (2021) [**49**] used lattice Boltzmann method with moment-based boundary conditions to compute flow in the slip regime. They imposed Navier-Maxwell slip conditions and Burnett-order stress conditions with the discrete velocity Boltzmann equation on stationary and moving boundaries. They studied Micro-Couette and micro-lid-driven cavity flows numerically at Knudsen and Mach numbers of the order $O(10^{-1})$.

Chapter 2

Problem description and mathematical modeling

2.1 Problem description

A two-dimensional fluid flow in a square cavity has been investigated in this present work with slip boundary conditions in the walls. The top wall (lid) is moving with a constant horizontal velocity u_o from left to right (i.e., positive x-direction) across the cavity while the other walls remain stationary. The model configuration and the boundary conditions are shown in Figure 2.1. In this problem the cavity fluid is incompressible in nature and the flow is assumed to be laminar. The physical properties of fluid are kept constant. Due to the dragging action of lid, fluid circulate inside the cavity.

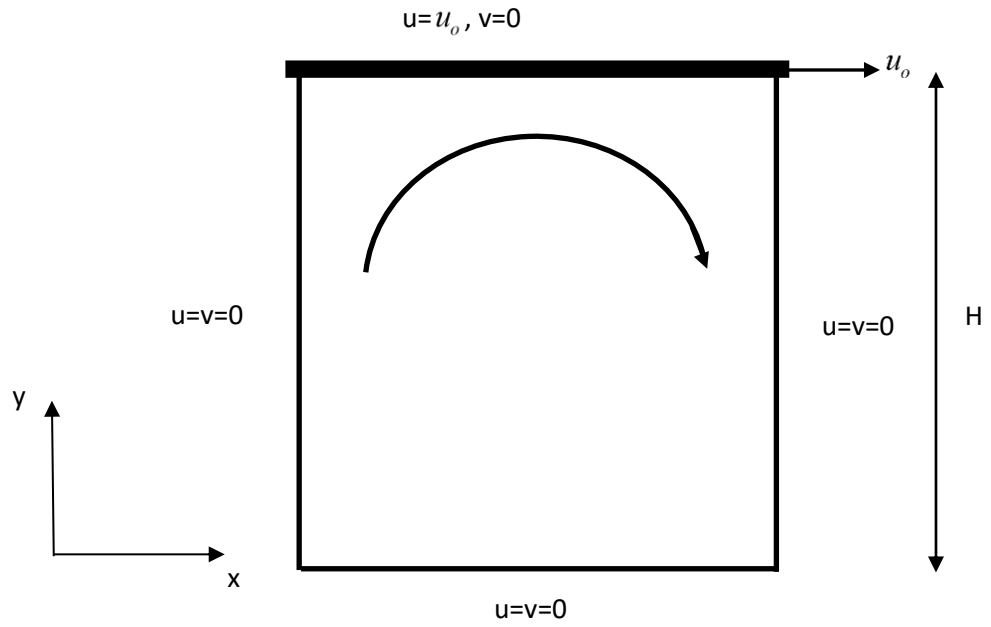

Fig. 2.1 A schematic of cavity flow driven by a moving horizontal wall in the xy-plane.

2.2 Governing equations

To express the conservation equations of mass and momentum, the following non-dimensional transformations are introduced.

$$\tilde{x} = \frac{x^*}{H},\ \tilde{y} = \frac{y^*}{H},\ \tilde{u} = \frac{u^*}{u_o},\ \tilde{v} = \frac{v^*}{u_o},\ \tilde{p} = \frac{p^*}{\rho u_o^2},\ \tilde{t} = \frac{t^* u_o}{H}$$

where, $\tilde{x}$ and $\tilde{y}$ are the dimensionless Cartesian co-ordinates, $\tilde{u}$ and $\tilde{v}$ are the dimensionless velocity components, $\tilde{t}$ and $\tilde{p}$ are dimensionless time and pressure. H is the height of the cavity and u_o indicates lid velocity. The non-dimensional form of the two-dimensional conservation equations for unsteady, Newtonian fluid flow with neglected viscous dissipation effect are given below

Continuity equation:

$$\frac{\partial \tilde{u}}{\partial \tilde{x}} + \frac{\partial \tilde{u}}{\partial \tilde{y}} = 0 \tag{2.1}$$

Neglecting the x-momentum gravitational term, the x-momentum equation can be expressed as

x-momentum equation:

$$\frac{\partial \tilde{u}}{\partial \tilde{t}} + \tilde{u}\frac{\partial \tilde{u}}{\partial \tilde{x}} + \tilde{v}\frac{\partial \tilde{u}}{\partial \tilde{y}} = -\frac{\partial \tilde{p}}{\partial \tilde{x}} + \frac{1}{Re}\left(\frac{\partial^2 \tilde{u}}{\partial \tilde{x}^2} + \frac{\partial^2 \tilde{u}}{\partial \tilde{y}^2}\right) \tag{2.2}$$

y-momentum equation:

$$\frac{\partial \tilde{v}}{\partial \tilde{t}} + \tilde{u}\frac{\partial \tilde{v}}{\partial \tilde{x}} + \tilde{v}\frac{\partial \tilde{v}}{\partial \tilde{y}} = -\frac{\partial \tilde{p}}{\partial \tilde{y}} + \frac{1}{Re}\left(\frac{\partial^2 \tilde{v}}{\partial \tilde{x}^2} + \frac{\partial^2 \tilde{v}}{\partial \tilde{y}^2}\right) \tag{2.3}$$

The pressure term in the momentum equations is dynamic pressure. The non-dimensional parameters appearing in the above momentum and equation under consideration is

$$Re = \frac{Hu_o}{\nu} \qquad \text{(Reynolds number)} \qquad (2.4)$$

where, ν is kinematic viscosity. The dimensionless number has been used to study the parametric behavior of the lid driven cavity fluid flow.

2.3 Physical boundary conditions

According to Maxwell first order slip model the velocity boundary conditions are given as follows:

$$u\big|_{y=H} = u_o - l_s \left.\frac{\partial u}{\partial y}\right|_{y=H} \qquad v\big|_{y=H} = 0 \qquad (2.5a)$$

$$u\big|_{y=0} = l_s \left.\frac{\partial u}{\partial y}\right|_{y=0} \qquad v\big|_{y=0} = 0 \qquad (2.5b)$$

l_s is the slip length represented as, $l_s = \frac{2-\sigma}{\sigma}\lambda$ Where σ is tangential momentum accommodation coefficient defined as:

$\sigma = \frac{\tau_i - \tau_r}{\tau_i - \tau_w}$, τ_i is the incident tangential momentum of fluid molecules and τ_r is the reflected tangential momentum of the fluid molecules. If $\tau_i = \tau_r$ i.e., $\sigma = 0$ is termed as Specular reflection and if $\tau_r = \tau_w$ (reflected molecules capture the property of the wall) i.e., $\sigma = 1$ termed as Diffuse reflection. σ ranges from 0 to 1. λ is the mean free path of the molecules.

2.4 Skin friction coefficient:

The distribution of skin-friction co-efficient (c_f) at the south wall of the cavity can be calculated as equation 14.

$$c_f = \frac{\mu \partial u / \partial y}{\frac{1}{2}\rho u_o^2} \tag{2.6}$$

Where, (μ) is the dynamic viscosity of fluid, (ρ) is the bulk density of fluid and u_o is the free stream velocity of the fluid. In this present work free stream velocity is equal to lid velocity u_o

.

Chapter 3

Numerical approach

3.1 Single Relaxation Time – Lattice Boltzmann method (SRT-LBM) and model formulation

In the present work SRT-LBM is used to study two-dimensional fluid flow patterns in a square cavity with slip boundary conditions. The lattice Boltzmann method is a mesoscopic method. This method has been proven suitable for microscopic flow simulation where system dimension is the order of mean free path of the particles. In this study we have used D2Q9 model.

Figure 3.1 is a schematic of the D2Q9 model which consists of one center node and eight neighbouring nodes. These nodes are connected with the lattice linkages. The evolution of the particle distribution function without the force term can be expressed by the colliding step Eq.(1) and the streaming step Eq.(2) of the lattice Boltzmann equation (Guo et al.,2002) [**45**]

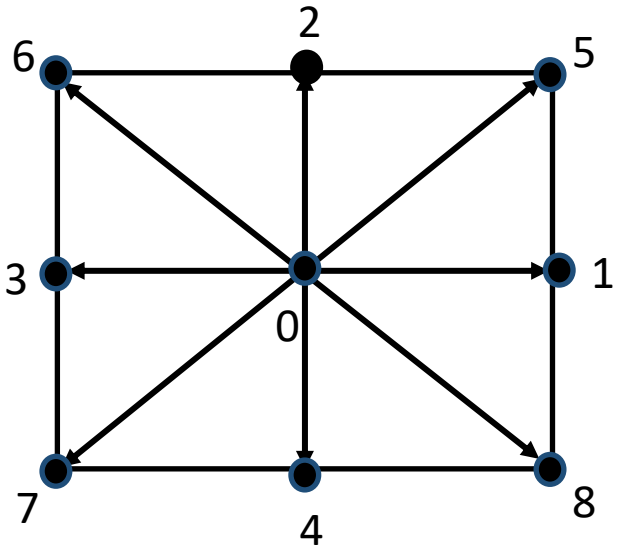

FIG. 3.1 Schematic diagrams of D2Q9 lattice used in this study

$$f_i^*(\vec{x},t) = f_i(\vec{x},t) - \frac{\Delta t}{\tau}(f_i(\vec{x},t) - f_i^{eq}(\vec{x},t)) \tag{3.1}$$

$$f_i(\vec{x} + \vec{c}_i\Delta t, t + \Delta t) = f_i^*(\vec{x},t) \tag{3.2}$$

In the standard D2Q9 model, the equilibrium distribution function can be expressed as [**46**]

$$f_i^{eq}(\vec{x},t) = \omega_i\rho\left[1 + \frac{\vec{c}_i \cdot \vec{u}}{c_s^2} + \frac{(\vec{c}_i \cdot \vec{u})^2}{2c_s^4} - \frac{\vec{u}^2}{2c_s^2}\right] \tag{3.3}$$

where $f_i(\vec{x},t)$ is the particle distribution function at position x and the time t, representing the number of particles moving with lattice velocity $\vec{c}_i$,and $f_i^*(\vec{x},t)$ represents the post-collision distribution function, and f_i^{eq} is the equilibrium particle distribution function , Δt is the time step, and τ is the dimensionless relaxation time, which can be expressed as

$$\tau = \frac{\nu}{c_s^2\Delta t} + \frac{1}{2} \tag{3.4}$$

Where ν is the kinematic viscosity, the speed of sound c_s is given by $c_s = \frac{c}{\sqrt{3}}$,where $c = \frac{\Delta x}{\Delta t}$, Δx is the lattice spacing. In the present work we set the lattice units with $\Delta x = \Delta t = 1$.

where $\vec{u}$ is the macroscopic velocity of fluid, and ρ is the macroscopic density. The discrete velocity $\vec{c}_i$ and the weight coefficient ω_i are given by

$$c_i = \begin{cases} (0,0) & i = 0 \\ c(\cos[(i-1)\pi/2], \sin[(i-1)\pi/2]) & i = 1,2,3,4 \\ \sqrt{2}c(\cos[(2i-1)\pi/4], \sin[(2i-1)\pi/4]) & i = 5,6,7,8 \end{cases}$$

$$\omega_i = \begin{cases} 4/9 & i = 0 \\ 1/9 & i = 1,2,3,4 \\ 1/36 & i = 5,6,7,8 \end{cases}$$

The local macroscopic density ρ and velocity $\vec{u}$ are computed by

$$\rho = \sum_i f_i \ , \qquad \rho\vec{u} = \sum_i \vec{c}_i f_i \tag{3.5}$$

The mesoscopic parameter relaxation time (τ) is related with the macroscopic kinematic viscosity (ν). The value of (τ) is very sensitive for accuracy and stability of the problem. The incompressibility limit has been performed under Mach number 0.3, depending on which all results are generated.

3.2 Slip boundary conditions

The slip boundary conditions of LBM were discussed in many published papers. The flow boundary conditions are described using the distribution functions at the boundary. At the boundary nodes, the outward distribution functions from the cavity are known from the streaming process and the inward distribution functions to the cavity are unknown. Figure 3 is the schematic of the distribution functions at the boundary nodes. The solid arrows of Figure 3.2 indicate the known distribution functions deriving from streaming, and the dotted arrows represent the unknown distribution functions.

In this present work flow field has investigated with two types of boundary condition namely TMAC (Tangential momentum accommodation coefficient) scheme and MBSR (Modified bounce back and specular reflection) scheme.

TMAC scheme: TMAC scheme i.e., the combination of bounce back and specular reflection is applied at the top moving boundary and the other three stationary boundaries. This method

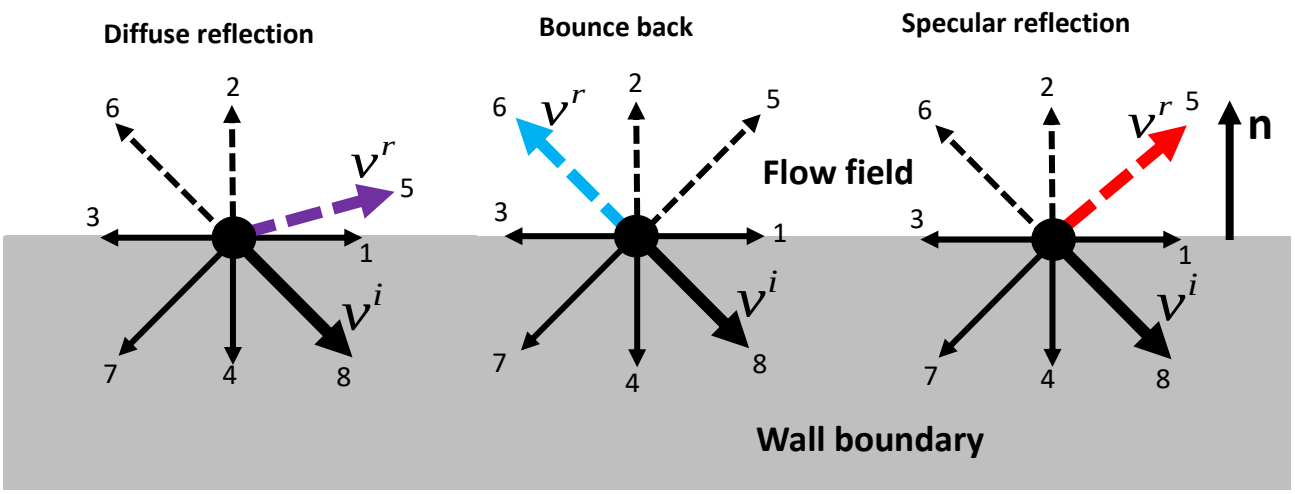

Fig. 3.2 Schematic diagram of fluid-wall (bottom) interactions and velocity direction of a two-dimesional D2Q9 model, where v^i is the incident velocity and v^r is the reflected velocity of fluid particles. Here, n is the normal direction towards the flow field. Dotted arrows indicates the unknown distributions and solid arrows indicates the known distributions.

incorporates the wall slip introducing σ with the boundary conditions. According to this scheme the unknown distribution functions can be calculated as follows [**43**]:

South wall (bottom) boundary conditions:

$$f_2(x,0) = f_4(x,0)$$

$$f_5(x,0) = \sigma f_7(x,0) + (1-\sigma) f_8(x,0) - \frac{\sigma}{2}\left[f_1(x,0) - f_3(x,0)\right] \tag{3.6}$$

$$f_6(x,0) = \sigma f_8(x,0) + (1-\sigma) f_7(x,0) + \frac{\sigma}{2}\left[f_1(x,0) - f_3(x,0)\right]$$

East (right) wall boundary conditions:

$$f_3(n,y) = f_1(n,y)$$

$$f_6(n,y) = \sigma f_8(n,y) + (1-\sigma) f_5(n,y) - \frac{\sigma}{2}\left[f_2(n,y) - f_4(n,y)\right] \tag{3.7}$$

$$f_7(n,y) = \sigma f_5(n,y) + (1-\sigma) f_8(n,y) + \frac{\sigma}{2}\left[f_2(n,y) - f_4(n,y)\right]$$

West (left) wall boundary conditions:

$$f_1(0,y) = f_3(0,y)$$

$$f_5(0,y) = \sigma f_7(0,y) + (1-\sigma) f_6(0,y) + \frac{\sigma}{2}\left[f_2(0,y) - f_4(0,y)\right] \quad (3.8)$$

$$f_8(0,y) = \sigma f_6(0,y) + (1-\sigma) f_7(0,y) - \frac{\sigma}{2}[f_2(0,y) - f_4(0,y)]$$

At the north (top) boundary the lid movement is expressed as

$$f_4(x,m) = f_2(x,m)$$

$$f_7(x,m) = \sigma f_5(x,m) + (1-\sigma) f_6(x,m) + \frac{\sigma}{2}\left[f_1(x,m) - f_3(x,m)\right] - \frac{\sigma}{2}\rho_N u_o \quad (3.9)$$

$$f_8(x,m) = \sigma f_6(x,m) + (1-\sigma) f_5(x,m) - \frac{\sigma}{2}\left[f_1(x,m) - f_3(x,m)\right] + \frac{\sigma}{2}\rho_N u_o$$

$$\rho_N = f_0(x,m) + f_1(x,m) + f_3(x,m) + 2\left[f_2(x,m) + f_6(x,m) + f_5(x,m)\right]$$

where, ρ_N is the density at the north boundary, u_0 is the x-component velocity, ‘ o ’, and ‘ m ’ indicate the first node of x axis and last node of the y axis respectively.

MBSR SCHEME: Wang et al. (2018) [**36**] modified the bounce back and specular reflection boundary condition proposed by Succi (2002) based on the Navier slip model. They deducted a relationship between the accommodation coefficient and the slip length with the halfway and the modified slip boundary conditions, under the framework of the lattice Boltzmann method (LBM). The proposed methods are more accurate than the approximately choosing

accommodation coefficients which gives flexibility in numerical simulations for different complex flows. According to the MBSR the boundary conditions at different wall with slip can be expressed as:

South wall (bottom) boundary conditions:

$$f_2(x,0) = f_4(x,0)$$

$$f_5(x,0) = \sigma f_7(x,0) + (1-\sigma) f_8(x,0) \tag{3.10}$$

$$f_6(x,0) = \sigma f_8(x,0) + (1-\sigma) f_7(x,0)$$

East (right) wall boundary conditions:

$$f_1(n,y) = f_3(n,y)$$

$$f_6(n,y) = \sigma f_8(n,y) + (1-\sigma) f_5(n,y) \tag{3.11}$$

$$f_7(n,y) = \sigma f_5(n,y) + (1-\sigma) f_8(n,y)$$

West (left) wall boundary conditions:

$$f_1(0,y) = f_3(0,y)$$

$$f_5(0,y) = \sigma f_7(0,y) + (1-\sigma) f_6(0,y) \tag{3.12}$$

$$f_8(0,y) = \sigma f_6(0,y) + (1-\sigma) f_7(0,y)$$

North (top) wall boundary conditions:

$$f_4(x,m) = f_2(x,m)$$

$$f_8(x,m) = \sigma f_6(x,m) + (1-\sigma) f_5(x,m) + \rho_N \sigma \frac{u_o}{6} \tag{3.13}$$

$$f_7(x,m) = \sigma f_5(x,m) + (1-\sigma) f_6(x,m) - \rho_N \sigma \frac{u_o}{6}$$

$$\rho_N = f_0(x,m) + f_1(x,m) + f_3(x,m) + 2\left[f_2(x,m) + f_6(x,m) + f_5(x,m)\right]$$

Where Wang et al. derived (the modification part they did) the following relation between accommodation coefficient (σ) and slip length (l_s) i.e.,

$$\sigma = \frac{1}{1 + \frac{l_s}{\tau}} \tag{3.14}$$

3.3 Maxwell First Order Slip Model

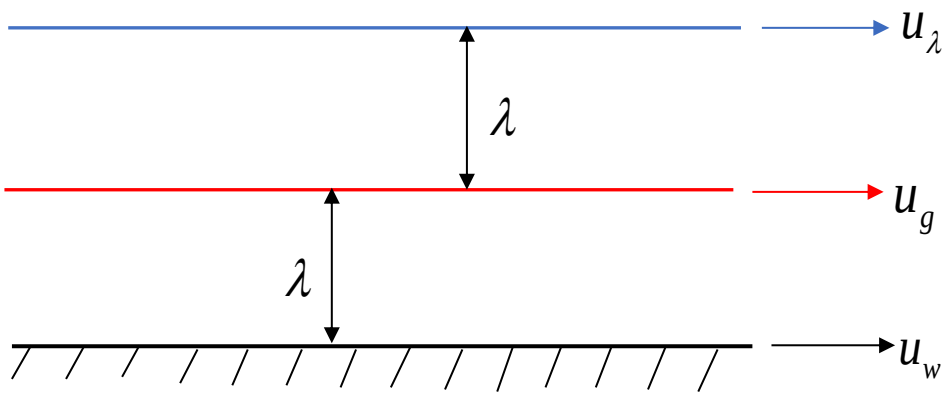

Fig.3.3 Schematic of different fluid layers

Let say solid boundary (Black colour line) move with a velocity u_w and there is a gas layer (Red colour line) where the fluid is moving with a velocity u_g. And the distance between the layers is assumed λ (mean free path) because in gas flow, the smallest resolution that can be captured is the molecular mean free path.

There is another layer (Blue colour line), this layer has a velocity u_λ.

Statistically in the mid layer half of the molecules can join from the top layer and half from the wall layer, so

$$u_g = \frac{1}{2}u_\lambda + \frac{1}{2}u_{reflected} \tag{3.15}$$

$u_{reflected}$ can have the property of the u_λ and u_w depending on whether it is specular reflection or diffuse reflection. So, the fraction or the probability of specular reflection is $(1-\sigma)$

So, equation (3.15) become

$$u_g = \frac{1}{2}u_\lambda + \frac{1}{2}\left[(1-\sigma)u_\lambda + \sigma u_w\right] \tag{3.16}$$

Where σ is tangential momentum accommodation coefficient defined as

$\sigma = \frac{\tau_i - \tau_r}{\tau_i - \tau_w}$, τ_i is the incident tangential momentum of fluid molecules and τ_w is the reflected tangential momentum of the fluid molecules. If $\tau_i = \tau_r$ i.e., $\sigma = 0$ is termed as Specular reflection and if $\tau_r = \tau_w$ (reflected molecules capture the property of the wall) i.e., $\sigma = 1$ termed as Diffuse reflection.

From the definition of gradient

$$\sigma(u_\lambda - u_w) = 2\lambda \left.\frac{\partial u}{\partial y}\right|_w$$

$$u_\lambda = u_w + \left.\frac{2\lambda}{\sigma}\frac{\partial u}{\partial y}\right|_w \tag{3.17}$$

Substituting equation(3.17) in equation (3.16) we get

$$u_g = \frac{2-\sigma}{2}u_w + \left.\frac{2-\sigma}{2}\frac{2\lambda}{\sigma}\frac{\partial u}{\partial y}\right|_w + \frac{\sigma}{2}u_w$$

Or $u_g = u_w + \left.\frac{2-\sigma}{\sigma}\lambda\frac{\partial u}{\partial y}\right|_w$

$\therefore u_g - u_w = u_{slip} = \left. l_s \frac{\partial u}{\partial y}\right|_w$ where l_s is known as slip length, $l_s = \frac{2-\sigma}{\sigma}\lambda$

According to above analysis the kinetic boundary condition in this present work is

$$u\big|_{y=H} = u_o - \left. l_s \frac{\partial u}{\partial y}\right|_{y=H} \tag{3.18}$$

$$u\big|_{y=0} = \left. l_s \frac{\partial u}{\partial y}\right|_{y=0} \tag{3.19}$$

3.4 Formulation of TMAC scheme:

In LBM fluid density is the summation of all distribution function, Zou & He (1997)

$$\rho = \sum_{i=0}^{i=8} f_i = f_0 + f_1 + f_2 + f_3 + f_4 + f_5 + f_6 + f_7 + f_8$$

$$f_2 + f_5 + f_6 = \rho - (f_0 + f_1 + f_3 + f_4 + f_7 + f_8) \tag{3.20}$$

In the above equation $f_2,\ f_5,\ f_6$ and ρ is unknown

From momentum conservation in x and y direction the following relations are found

$$f_5 - f_6 = \rho u_x - (f_1 - f_3 + f_8 - f_7) \tag{3.21}$$

$$f_2 + f_5 + f_6 = \rho u_y + (f_4 + f_7 + f_8) \tag{3.22}$$

Combining equation (5) & (7) the unknown quantity ρ can be calculated as

$$\rho = \frac{\left[f_0 + f_1 + f_3 + 2(f_4 + f_7 + f_8) \right]}{1 - u_y}$$

There are four unknowns and three equations that means system still not closed so, an assumption is taken here that is the Bounce back of the non-equilibrium part of the particle distribution normal to the boundary

$$f_i^{neq} = f_i - f_i^{eq}$$

$$f_2 - f_4 = f_2^{eq} - f_4^{eq}$$

From equilibrium distribution function formula and using the values $\vec{c}_2(0,1), \vec{c}_4(0,-1)$ and $\vec{u}(u_x, u_y)$ the following equations can be obtained

$$f_2^{eq} = w_2\rho\left[1+3u_y+\frac{9}{2}u_y^2-\frac{1}{2}(u_x^2+u_y^2)\right] \tag{3.23}$$

$$f_4^{eq} = w_4\rho\left[1-3u_y+\frac{9}{2}u_y^2-\frac{1}{2}(u_x^2+u_y^2)\right] \tag{3.24}$$

Now substituting equation (8) from equation (9) and using the corresponding weight coefficient for D2Q9 lattice, $w_2 = w_4 = \frac{1}{9}$ the unknown distribution f_2 can be calculated as follows

$$f_2 = f_4 + \frac{2}{3}\rho u_y$$

Now using above relation and adding equations (6) & (7) the other two unknown distributions in terms of known distribution can be calculated as follows

$$f_5 = f_7 + \frac{1}{2}\left[\rho u_x - (f_1 - f_3)\right] + \frac{1}{6}\rho u_y \quad \&$$

$$f_6 = f_8 - \frac{1}{2}\left[\rho u_x - (f_1 - f_3)\right] + \frac{1}{6}\rho u_y$$

Incorporation of slip using tangential momentum accommodation co-efficient (σ)

From physics of collision of particle in solid wall, tangential accommodation coefficient can be defined as

$$\sigma = \frac{\rho_R U_R - \rho_I U_I}{\rho_R U_W - \rho_I U_I}$$

ρ_I and ρ_R is the density of the incident and reflected particles respectively. U_I, U_R and U_W represents the tangential velocity of the incident particles, reflected particles and of the wall respectively. And considering ρ and U as the overall average density and tangential velocity of the fluid respectively the following relation can be written as follows

$$\rho = \rho_I + \rho_R$$

$$\rho U = \rho_I U_I + \rho_R U_R$$

From the mass conservation and to avoid particle accumulations on the boundaries, the reflected fluid should be equal to the incident fluid for an impermeable boundary. Therefore,

$$\rho_I = \rho_R = \frac{\rho}{2}$$

$$\sigma = \frac{U_R - U_I}{U_W - U_I}$$

$$U = \frac{1}{\rho}(\rho_I U_I + \rho_R U_R) = \frac{1}{2}\sigma U_W + (1 - \frac{\sigma}{2})U_I$$

In order to consider the effect of the permeation, and to describe the effects of the boundary on the tangential momentums with the macroscopic quantities, e.g., ρ and U ,a modified tangential momentum accommodation coefficient, σ' was proposed by Kuo and Chen (2008).

$\sigma' = \frac{U - U_{SR}}{U_W - U_{SR}}$ where U_{SR} is the average tangential velocity under the specular reflection by the impermeable boundary, which is equal to U_I .

So, the tangential momentum change of the fluid caused by the boundary can be also determined by

$$\rho(U - U_{SR}) = \sigma'\rho(U_W - U_{SR})$$

If U_{SR} can be expressed by the Taylor expansion at the wall about one mean free path (λ) away

$$U_{SR} \approx U + \lambda \left.\frac{\partial U}{\partial n}\right|_w + ...,$$

then the slip velocity, $U - U_W$, can be calculated by

$$U - U_W \approx \frac{1-\sigma'}{\sigma'} \lambda \left.\frac{\partial U}{\partial n}\right|_w$$

For a boundary with given σ' and the permeation velocity U_P ,the unknown distributions of the boundary nodes are contributed from three parts:

$$f_i = f_i^{sr} + f_i^{w} + f_i^{p}$$

f_i^{sr}, f_i^w and f_i^p indicates specular reflection, stress exerted by the wall and permeation condition respectively.

Specular reflection distributions are:

$$f_2^{sr} = f_4$$
$$f_5^{sr} = f_8$$
$$f_6^{sr} = f_7$$

From momentum conservation we get,

$$\rho U_{SR} = f_1 - f_3 + 2(f_8 - f_7)$$

The shear stress exerted by the wall leads to the momentum change

$$\sigma'\rho(U_W - U_{SR}) = \sum(f_i^w c_i)_x = f_5^w - f_6^w$$

$$\sum(f_i^w c_i)_y = f_2^w + f_5^w + f_6^w = f_5^w + f_6^w = 0$$

$f_2^w = 0$, because this distribution is in the normal direction towards the fluid from wall.

$$\therefore f_5^w = -f_6^w$$

$$f_5^w = \frac{\sigma'}{2}\rho(U_W - U_{SR})$$

If the wall is permeable and the permeation velocity, $U_P = U_Y$ is known then

$$\rho U_P = \sum(f_i^p c_i)_y = f_2^p + f_5^p + f_6^p$$

$$\sum(f_i^p c_i)_y = f_5^p - f_6^p = 0$$

$$\therefore f_5^p = f_6^p$$

Now from bounce back of non-equilibrium part

$$f_2^p = f_4^p + \frac{2}{3}\rho U_y$$

Here, $f_4^p = 0$ as it is not in the direction of fluid

$$\therefore f_2^p = \frac{2}{3}\rho U_y$$

From momentum conservation in normal direction we get,

$$\rho U_y = f_2^p + 2 f_5^p \tag{3.25}$$

Substituting f_2^p value in the above equation we get,

$$f_5^p = f_6^p = \frac{1}{6}\rho U_y$$

Now substituting f_2^{sr}, f_2^p and f_2^w values the unknown distribution f_2 can be calculated as follows

$$f_2 = f_2^{sr} + f_2^w + f_2^p$$

$$f_2 = f_4 + \frac{2}{3}\rho U_y \tag{3.26}$$

Similarly, the unknown distribution f_5 and f_6 is calculated as follows

$$f_5 = \sigma' f_7 + (1-\sigma') f_8 + \frac{\sigma'}{2}\left[\rho U_W - (f_1 - f_3)\right] + \frac{1}{6}\rho U_y \tag{3.27}$$

$$f_6 = \sigma' f_8 + (1-\sigma') f_7 - \frac{\sigma'}{2}\left[\rho U_W - (f_1 - f_3)\right] + \frac{1}{6}\rho U_y \tag{3.28}$$

3.5 Code validation and grid independence test

To solve the present problem, a FORTRAN SRT-LBM code has been developed and ran on Intel Corei5 processor. The grid independence study is performed for the present work considering different number of lattice grids. For TMAC and MBSR scheme, four sets of lattice grids 101x101, 201x201, 251x251 and 301x301 are used to check the grid independence as shown in Figure (3.4).

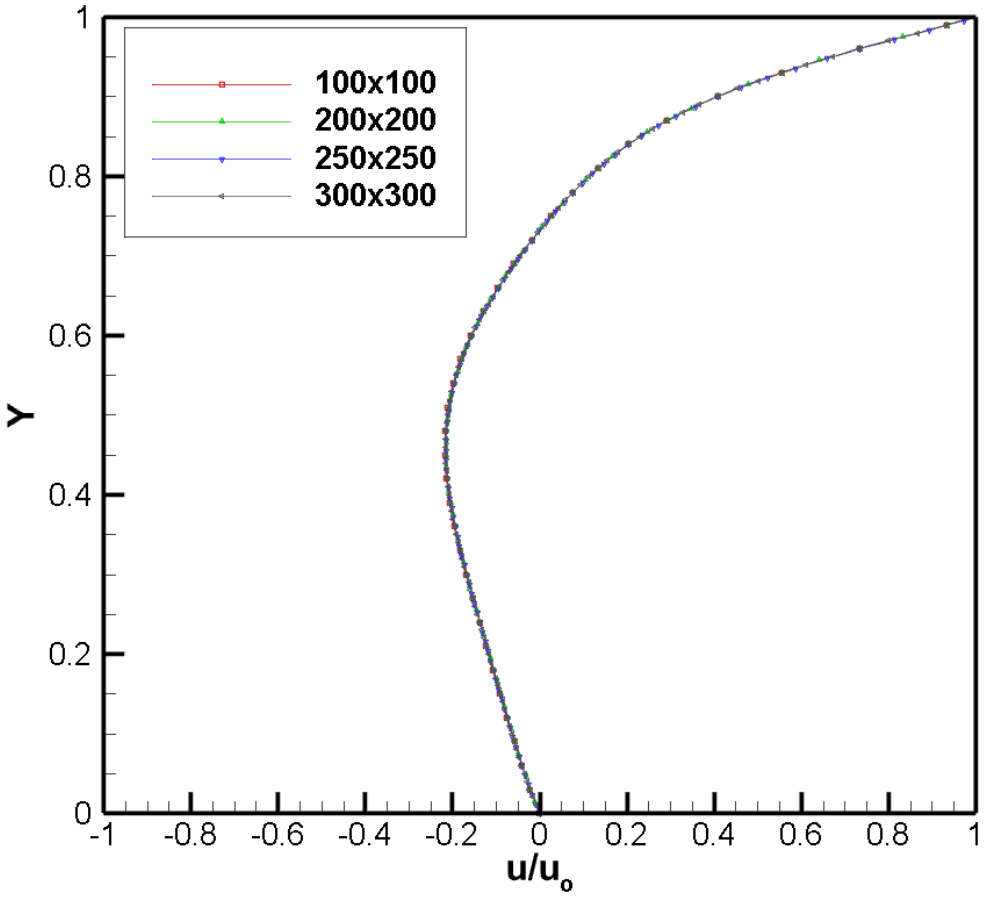

Fig.3.4 Grid independency test

As Table I shows CPU time is considerably less in case of grid size 201x201 compared to grid size 301x301, all subsequent calculations in the study are carried out with grid size 201x201.

TABLE I. Grid independence study

Mesh Size	CPU Time (s)
101x101	482.166
201x201	1725.476
251x251	2337.917
301x301	3169.122

The code validation is performed as shown in Figure (3.5) which shows a comparison between present study and the benchmark problem presented by Marchi et al. (2009) [**47**]. Here the comparison has been performed in terms of centerline variation of u and v velocity components in y and x direction respectively at Reynolds number 100. The mesh comprising of 201 x 201 lattices is finally used for the simulation purpose and the result shows a good agreement with the benchmark solution.

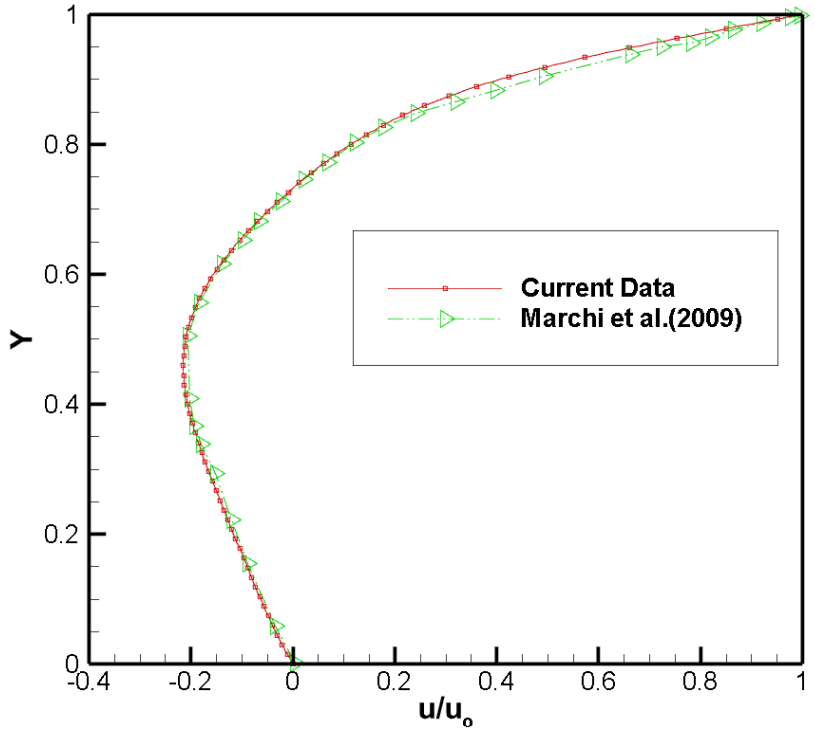

(a)

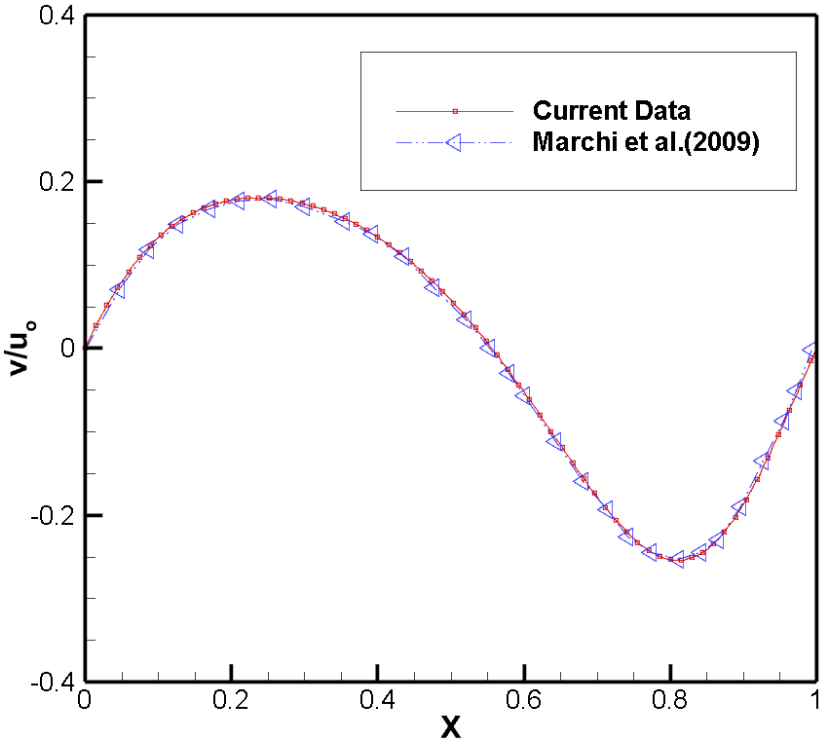

(b)

Fig.3.5 Comparison with Marchi et al. (2009) benchmark numerical solution at Re=100: (a) Centerline u-velocity profile, (b) Centerline v-velocity profile.

Chapter 4

Results and discussion

The present study describes the flow phenomena in a top lid driven square cavity providing slip boundary condition at all walls. The simulation is performed considering 201x201 lattice nodes in D2Q9 lattice structure. The numerical computation has been done based on Bhatnagar- Gross-Krook lattice Boltzmann model (BGK-LBM) using single relaxation time. Investigation of liquid flow in a lid driven cavity under slip condition has been studied over a wide range of Reynolds number (Re) $20 \le \mathrm{Re} \le 300$. The effect of slip velocity on the flow field through the slip boundary has been studied considering tangential momentum transfer at the boundary wall varying the accommodation coefficient (σ) $0.01 \le \sigma \le 1$ from maximum slip to close of no-slip. The graphical results in the present framework are obtained after steady state is attained. The subsequent sections describe the flow characteristics with the variation of slip parameter at different Re using streamlines, velocity profiles, and skin friction coefficient. A numerical comparison has been examined between MBSR and TMAC scheme for liquid flow lid driven cavity problem discussing deviation of numerical slip and requirement of computational time.

4.1 Effect of Reynolds number on slip flow

A detail investigation in the lid driven cavity under slip boundary condition has been incorporated using streamline map with the variation of Re which is shown in Fig. 4.1 through Fig. 4.5 The figures are arranged based on an examination of flow behavior according to slip parameter (accommodation coefficient, σ) indicating maximum slip (σ=0.01) to no-slip (σ=1) values. It is seen from the figures that the numerical simulations show clockwise circulatory pattern of the streamlines in general which occupy larger part of the cavity. Lid movement

occurs from left to right in positive x-direction at the top wall which leads a typical configuration of fluid flow for both the combination of shearing action with slip velocity.

Figure 4.1 through 4.5 depicts that the adjacent flow near the top wall moves faster along the positive x-direction before obstruction by the right wall. The strength of the fluid momentum is reduced close to the right wall and is guided by the same wall tends to flow downwards. The primary observation based on the effect of slip boundary condition to the no-slip boundary condition can be distinguished using contour map in the Fig. 4.1 to Fig. 4.5.

Figure 4.1 and 4.2 represent a family of streamlines for $\mathrm{Re} = 20$ and $\mathrm{Re} = 50$ respectively. The numerical simulation has been performed taking different σ values. The importance of slip parameter σ expands the study related to maximum slip through no-slip condition in the lid driven cavity which has been shown in Fig. 4.1(a) through Fig. 4.1(e). Figure 4.1(a) and Fig. 4.1(b) represents a formation of single clockwise circulation vortex in the cavity while a secondary vortex is formed in Fig. 4.1(c) to Fig. 4.1(e). More slip includes a greater effect of the tangential viscous stress to the fluid which dominates the shear action due to mechanical friction followed by the lid driven wall. The perturbation of flow in terms of secondary vortex due to the dominance of friction has been arisen in the enclosure as slip decreases which are shown in Fig. 4.1(d) to 4.1(e).

Fig. 4.2(a) and 4.2(b) exhibits similar tendency of the flow circulation in the enclosure at Re=50 in which a primary vortex is generated when σ values are 0.01 and 0.05 and main vortex breaks and generate a secondary counter clockwise vortex at the right bottom corner of the cavity which is presented in Fig. 4.2(c) through Fig. 4.2(e). The perturbation is attributed to the frictional dominance in the fluid which weakens the strength of the primary vortex as earlier mentioned. It is seen from the Fig. 4.1 and Fig. 4.2 that interesting changes happen in the flow field in which slip velocity plays an effective role and the lid effect becomes powerless with

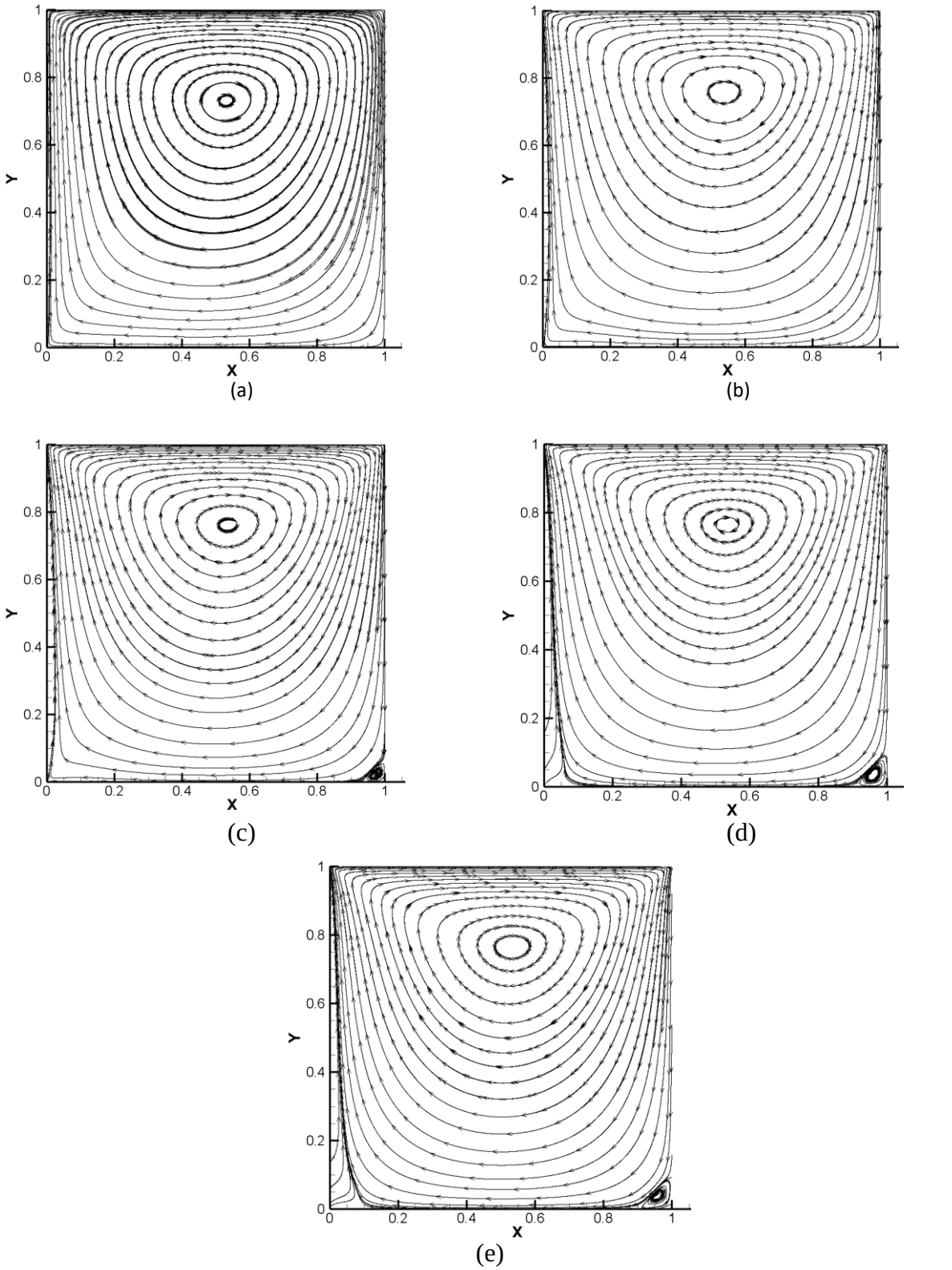

Fig.4.1 Streamlines plot at **Re=20** for various σ: (a) $\sigma = 0.01$, (b) $\sigma = 0.05$ (c) $\sigma = 0.1$, (d) $\sigma = 0.5$, (e) $\sigma = 1$

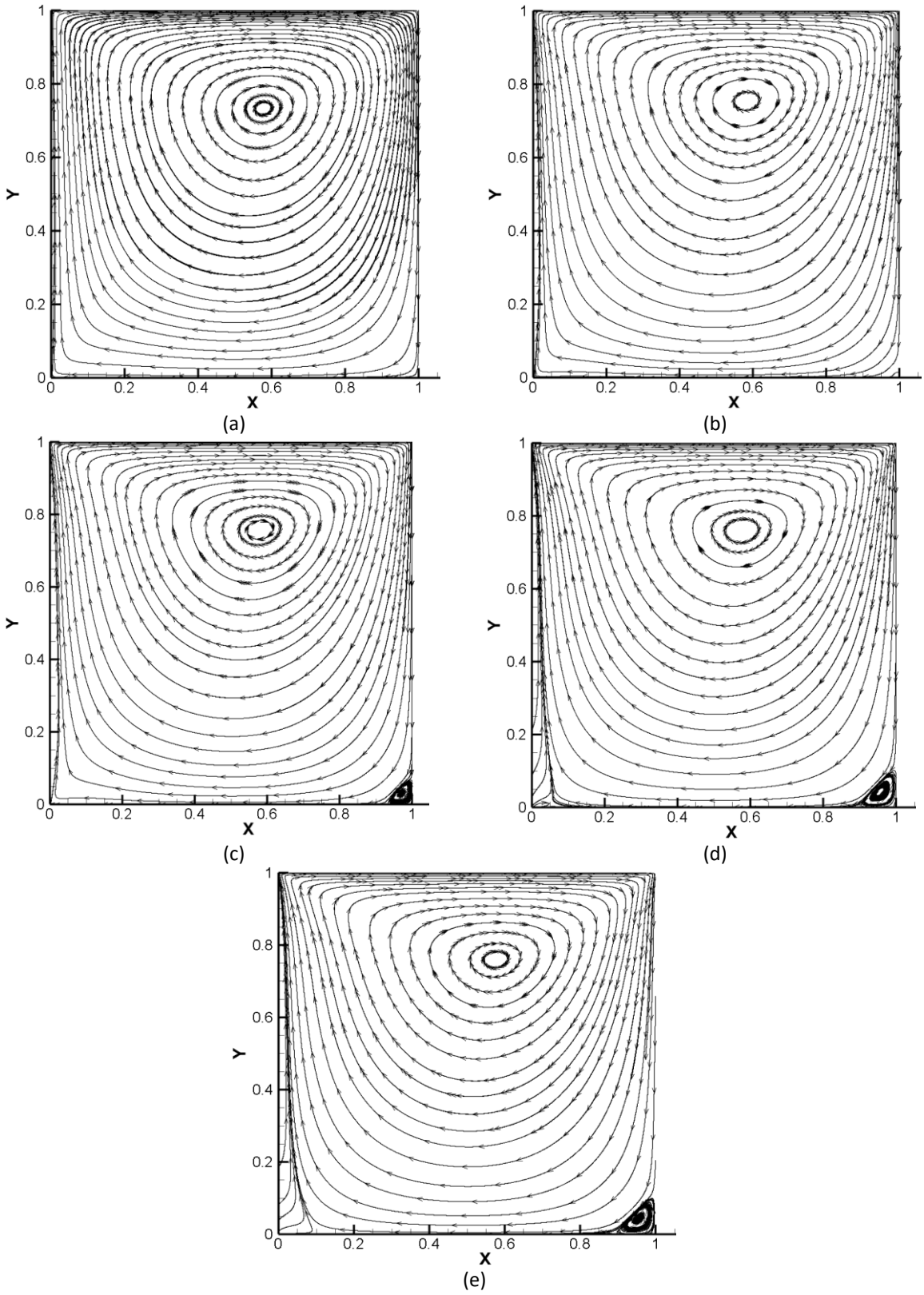

Fig.4.2 Streamlines plot at **Re=50** for various σ: (a) $\sigma = 0.01$, (b) $\sigma = 0.05$, (c) $\sigma = 0.1$, (d) $\sigma = 0.5$, (e) $\sigma = 1$

the increasing of slip parameter value in terms of σ. Figure 4.3 describes the effect of partial slip in the fluid at Re =100. At high Re the slip will completely eliminates the shear effect at σ value 0.01 which is pointed out in Fig. 4.3(a). As the accommodation coefficient increases to no-slip value (σ=1) a secondary vortex appears in the right bottom corner in the cavity which is revealed in Fig. 4.3(b) through 4.3(e). The primary vortex occupies the core of the main cell and local perturbation appears close to the bottom right wall due to the presence of frictional dominance over slip which weakening the vortex strength and circulates anticlockwise. The region of streamlines of secondary vortex grows with the increasing of slip parameter values indicating the more shear effect due to the presence of lid driven wall. It is seen from figures 4.4 (a) through 4.4(e) that slip is affecting the appearance of secondary vortex in the right bottom corner of the cavity at Re=300. In Fig. 4.4(a) when slip is maximum setting the σ value 0.01, a secondary vortex does not appear close to the right bottom corner because slippage provides higher velocity gradient, low wall friction and higher mass flow rate inside the boundary layer in the vicinity of the walls. As slip reduces i.e., σ increase, it is seen from figure 4.4(b) that the first trace of secondary vortex is found at σ value 0.05 adjacent to the right bottom corner due to adverse pressure gradient. Wall friction and stagnation pressure at this position encourage to form a secondary eddy in which the flow circulation is in anticlockwise direction. Figures 4.4(c) through 4.4(e) indicate the presence of secondary vortex and subsequently growth of the vortex as slip reduces.

A systematic observation has been done in order to provide additional information of the contour map of the streamlines has been presented in Table 1. The nature of fluid flow with the alternation of slip parameter from 0.01 to 1 mentioning the location of primary vortex center at different Re is shown in Table 1. Observing the primary vortex position from Table 1 it is elucidated that the dominance of shear action plays a significant role adjacent to the

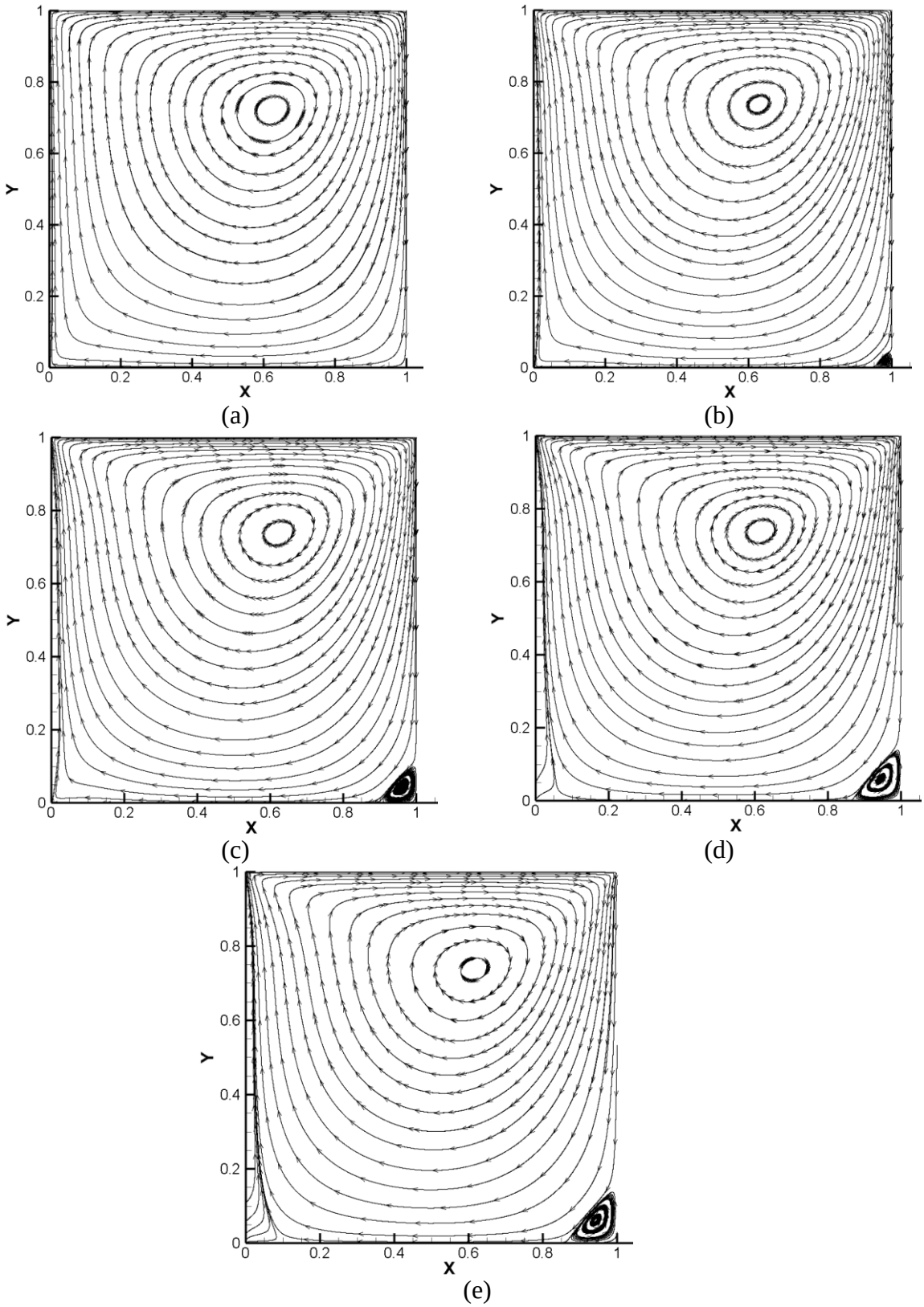

Fig.4.3 Streamlines plot at **Re=100** for various σ: (a) $\sigma = 0.01$, (b) $\sigma = 0.05$, (c) $\sigma = 0.1$, (d) $\sigma = 0.5$, (e) $\sigma = 1$

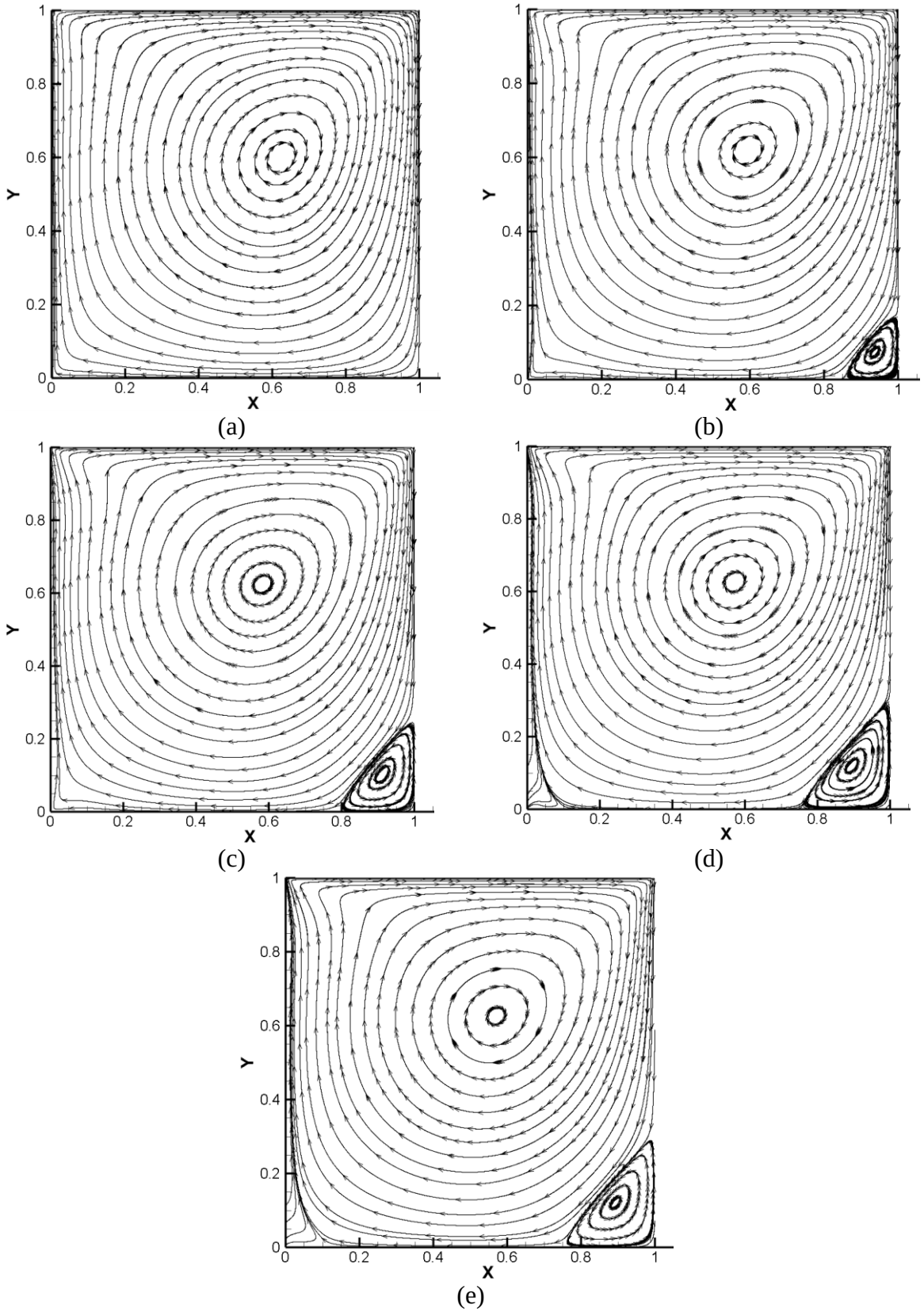

Fig.4.4 Streamlines plot at **Re=300** for various σ: (a) $\sigma = 0.01$, (b) $\sigma = 0.05$, (c) $\sigma = 0.1$, (d) $\sigma = 0.5$, (e) $\sigma = 1$.

upper region of the cavity and it penetrates through the fluid layers from top to near bottom with the variation of σ values from 0.01 to 1 as Re increases. Several numerical investigations and observations predict that as the slip increases the primary vortex center shifts towards the center of the cavity.

4.2 Velocity profiles with different slip parameter (σ) at different Reynolds number

Velocity vector comprises of two velocity components in terms of x-component velocity in the horizontal direction and y-component velocity at the vertical direction with respect to normal velocity direction. Fig. 4.5 to Fig. 4.9 describes the x-component as well as y-component velocity plots varying σ values at different Re. The x-component velocity profile at the vertical mid plane $x = 0.5$ has been shown in the Fig. 4.5(a) to 4.9(a) followed by increasing Re from top to bottom with varying σ values from 0.01 to 1. Component analysis of velocity vector at the point of intersection with the plane at $x = 0.5$ shows that the u-velocity is maximum and equal to lid velocity in the region adjacent to the top lid when $\sigma = 1$ that is the no slip boundary condition at the lid surface. The Figs. 4.5 through 4.9 show that when σ is not equal to 1 owing to slip boundary condition the u-velocity component of the adjacent layers near top wall and bottom wall is not equal to wall velocity, there is net relative motion (slip) between the walls and the fluid layers just adjacent to the walls. The figures describe that u-velocity decreases gradually as y decreases up to a certain depth as the evidence of the corresponding streamline plot. As the upper fluid domain is mainly dominated by shear force due to lid movement, fluid layers near the top boundary show positive u-velocity and near the center of the cavity there is negative x-velocity due to change of flow direction from right to left about the mid plane. The effect of partial slip parameter towards the maximum slip (σ values 0.5 to 0.01) is effective to suppress the u and v-component velocities which is depicts in Figs. 4.5 through 4.9. A partial slip is

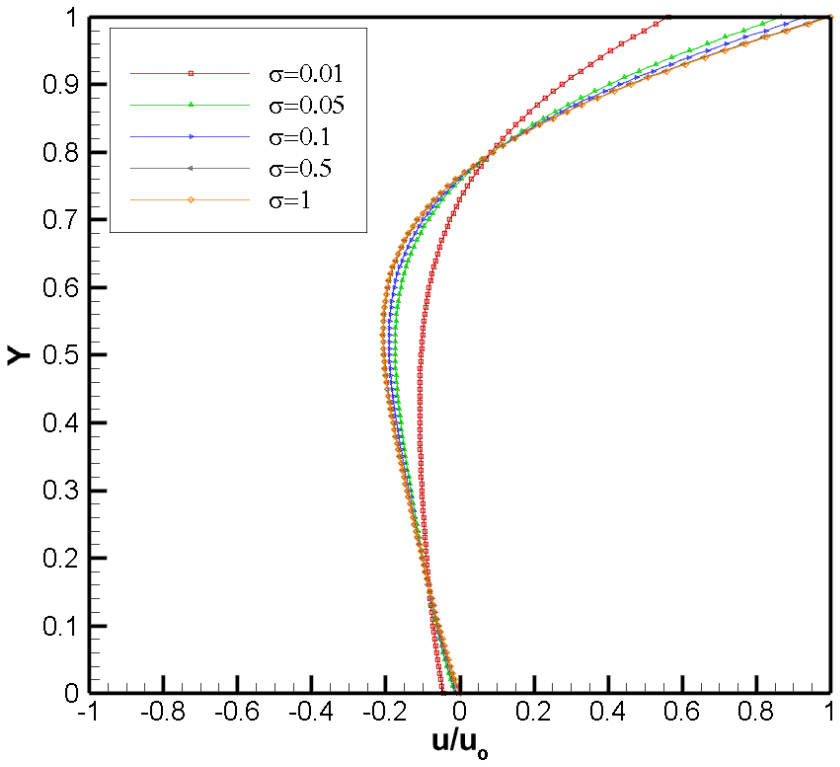

(a)

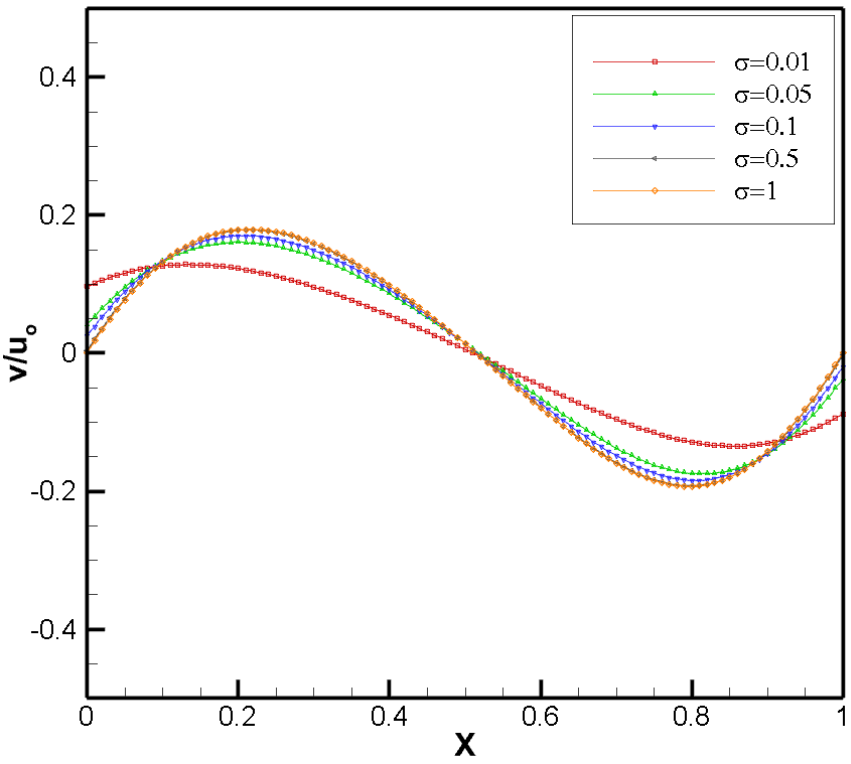

(b)

Fig. 4.5 Centerline u and v velocity profile along y and x axis respectively at **Re=20**

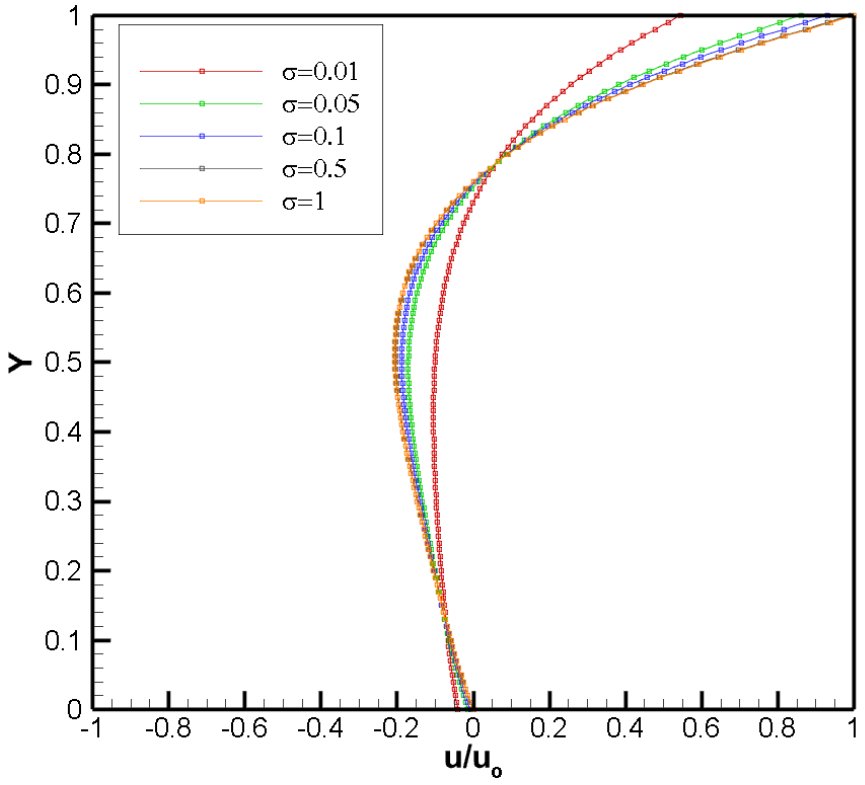

(a)

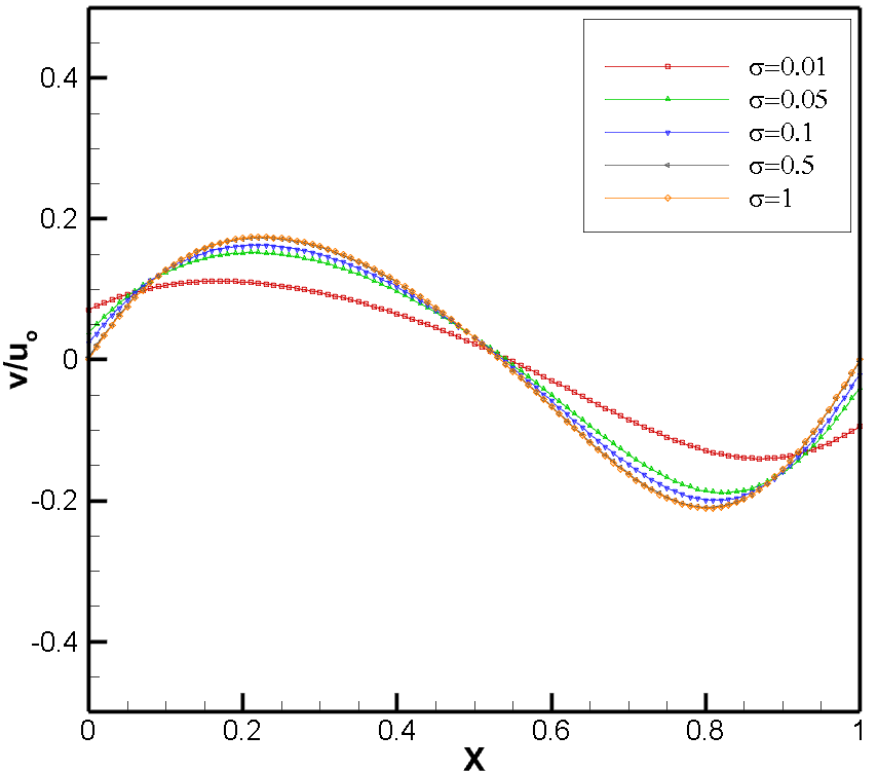

(b)

Fig. 4.6 Centerline u and v velocity profile along y and x axis respectively at **Re=50**

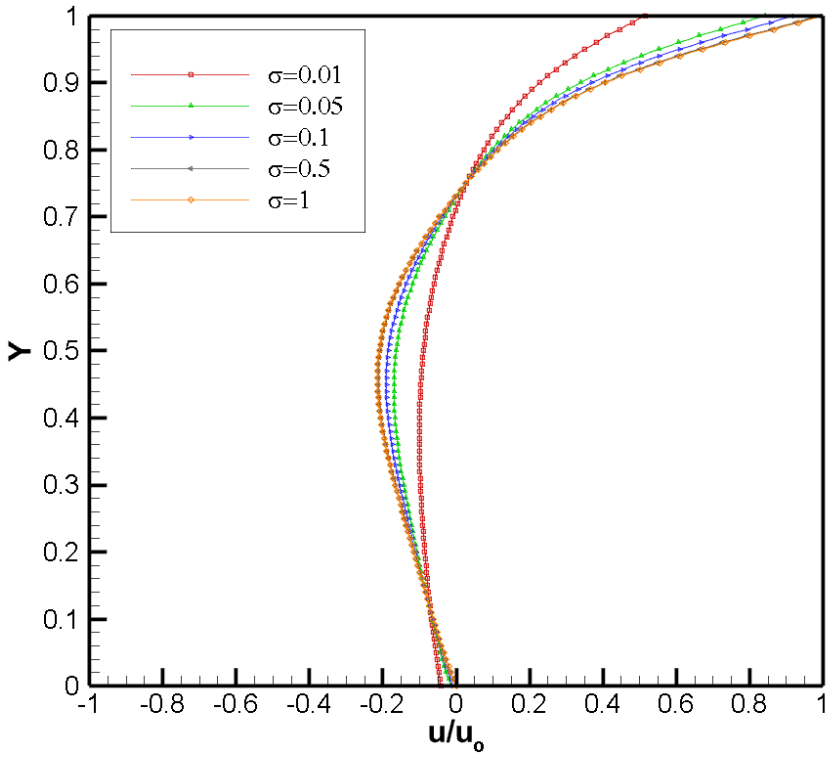

(a)

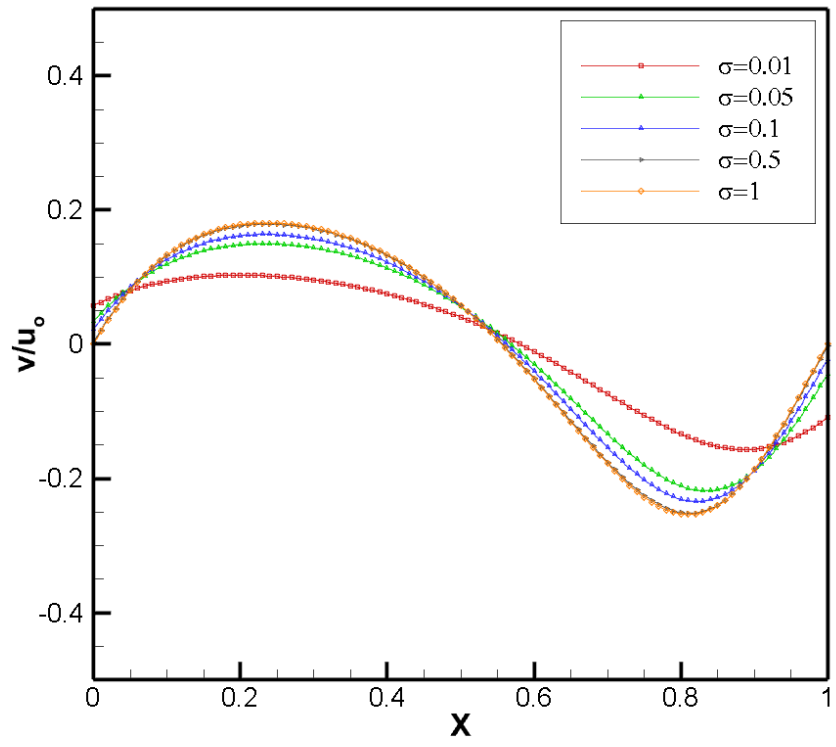

(b)

Fig. 4.7 Centerline u and v velocity profile along y and x axis respectively at **Re=100**

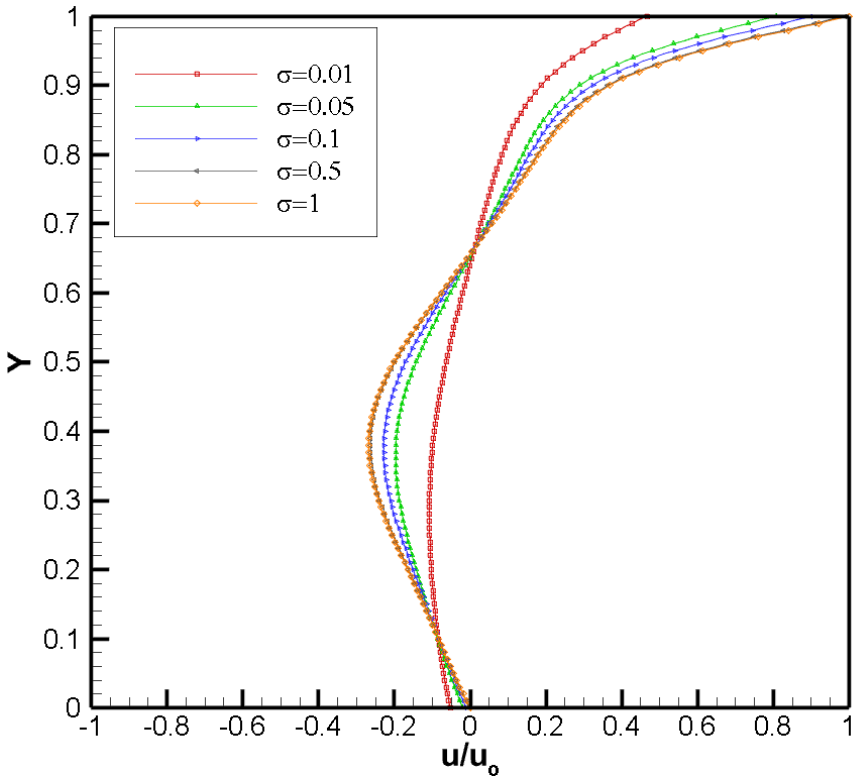

(a)

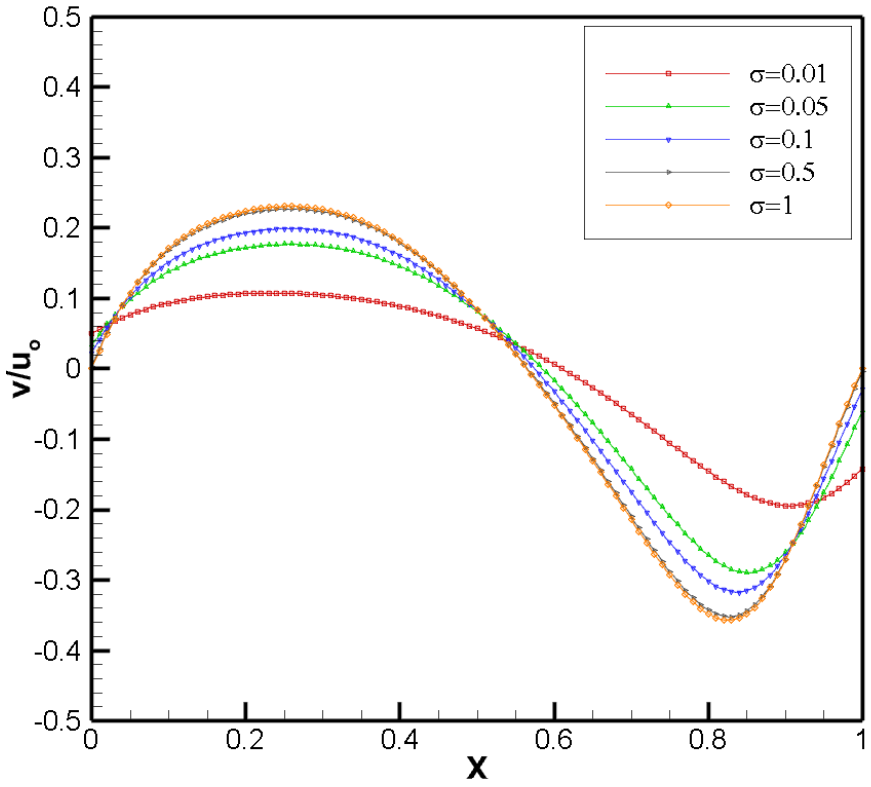

(b)

Fig. 4.8 Centerline u and v velocity profile along y and x axis respectively at **Re=200**

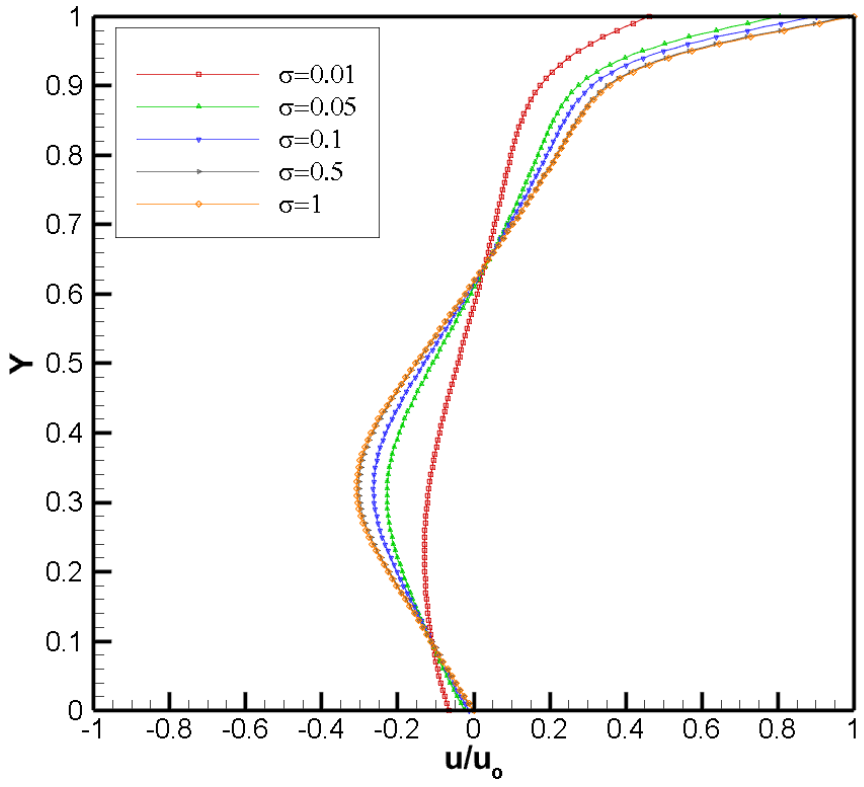

(a)

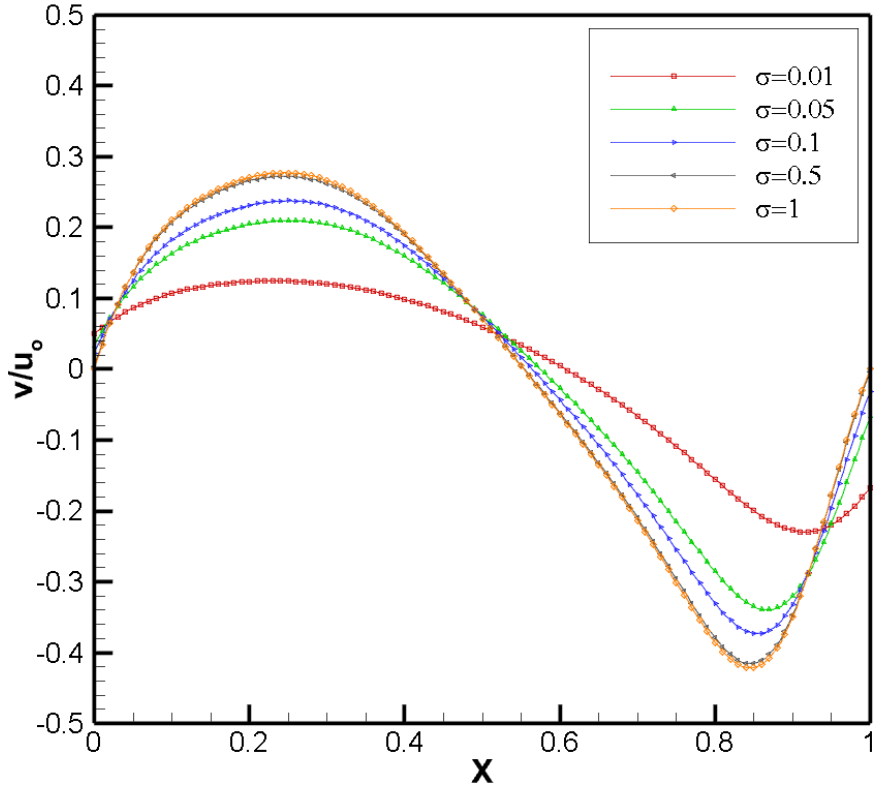

(b)

Fig. 4.9 Centerline u and v velocity profile along y and x axis respectively at **Re=300**

originated at a σ value 0.01 and the x-component velocity and y-component velocity deviates from the no-slip zero velocity value as partial slip slightly eliminate the mechanical friction generated by the moving wall. Fig. 4.5(a) to 4.9(a) for σ value 0.01 describes the x and y-component velocity deviation from the no-slip condition reduce with the increase of Re. It is seen from the Fig. 4.5 to Fig. 4.9 that as slip increases the magnitude of negative x-velocity reduces significantly about the mid plane at $x = 0.5$.

4.3 Effect of Reynolds number on slip at $\sigma = 0.01$ (maximum slip)

As from the previous study from Fig. 4.5 to Fig. 4.9 it is observed that maximum slip (σ=0.01) incorporates a significant change in x-component and y-component velocity compare to the other σ values. A more detail explanation is required to describe the effect of Re on maximum slip considering σ=0.01. Figure 4.10 (a) and 4.10(b) represent the effect of Re on slip through centerline x-component velocity and y-component velocity variation in the mid plane at $x = 0.5$ and $y = 0.5$ respectively. It is seen from Fig. 4.10(a) that the x-component velocity is higher for low Re (Re=20) compare to the rest of the Re values because of the relative motion of the subsequent top layer is less and with the increase of Re the relative motion between the adjacent layer of the top wall more which incorporate more slip in the flow. The tangential fluid velocity due to slip at the wall dominates over the normal x-direction wall velocity and shows more slippage effect for higher Re values compare to the lower one. The dominance of tangential fluid velocity over the wall movement increases as Re increases. Similarly at the bottom wall the slippage effect is more at higher Re compare to the other Re values which appears as negative x-component velocity near the bottom wall. Fig. 4.10(b) describes the y-component velocity profiles at different Re. According to the Fig. 4.10(b) the partial slip effect near the left wall is different from the

right wall. Adjacent to the left wall slippage occur mainly due to the direction of the relative fluid velocity at the vicinity of the left wall towards

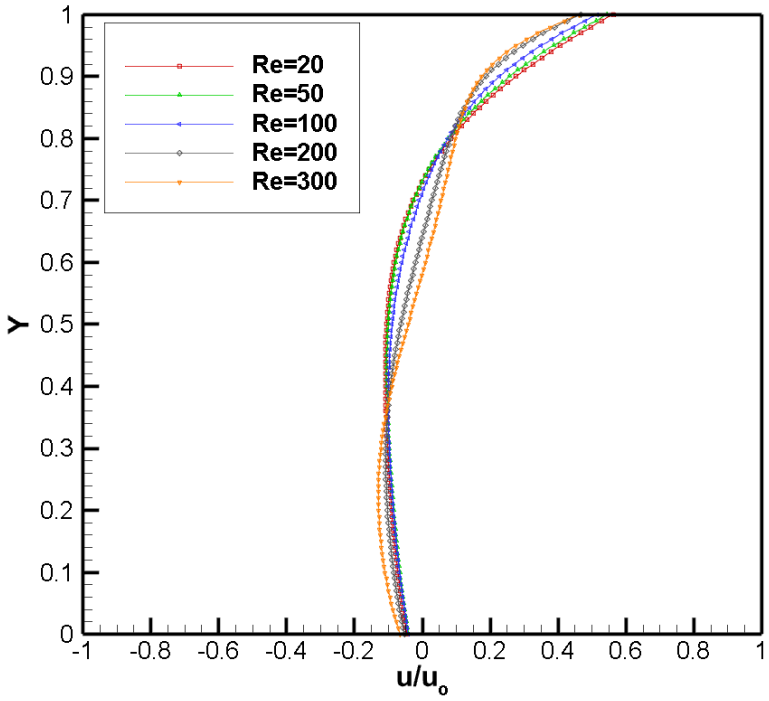

(a)

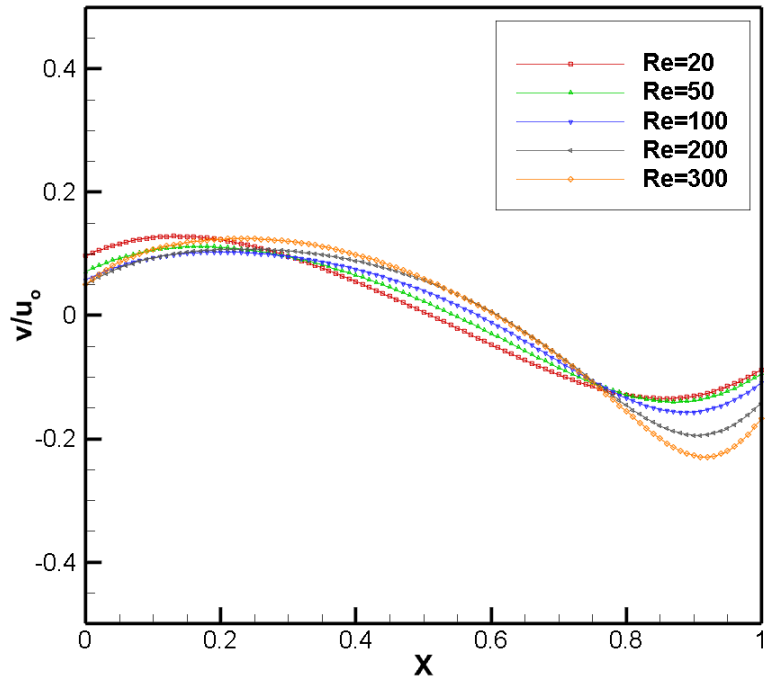

(b)

Fig. 4.10 Effect of Reynolds number on slip at $\sigma = 0.01$ in TMAC scheme.

the positive y-direction. A different phenomenon occurs near the right wall of the cavity where the relative motion between the right wall and its adjacent wall is flowed towards the negative y-direction. The results confirms that slip increases as the Re number increases because fluid layers gain higher velocity. It is also seen that as Re number increases the magnitude of negative x-velocity reduces.

4.4 Comparison of Modified Bounce Back with specular Reflection Scheme (MBSR) and Tangential Momentum Accommodation Coefficient Scheme (TMAC)

A comparison has been made based on two boundary conditions scheme in lattice Boltzmann (LB) simulation. Modified bounce back with specular reflection (MBSR) scheme and tangential momentum accommodation coefficient boundary scheme have been used to perform a numerical comparison based on deviation of numerical slip and the computation time in liquid flow lid driven cavity. In corporation of tangential momentum transfer to the wall in TMAC scheme as well as the determination of slip velocity using MBSR scheme has been discussed with its merits and demerits in reference [**48**]. In the present framework the comparison has been made on these two well-known boundary schemes for liquid filling cavity with lid movement. Figure 4.11 shows the u and v velocity profiles for $\mathrm{Re} = 50$ and $\mathrm{Re} = 200$ at mid plane for $\sigma = 0.01$ (maximum slip) using the slip boundary conditions, TMAC and MBSR boundary schemes. A similar comparison has been made for $\mathrm{Re} = 50$ and $\mathrm{Re} = 200$ at mid plane for $\sigma = 0.1$ which is given in Fig. 4.12. It is observed from Fig. 4.11 and Fig. 4.12 that MBSR scheme induces more numerical slip than TMAC scheme as reported in [**48**]. It is also seen from the Figs. 4.11 (a) and Figs. 4.11(c) that the slippage effect is more in for lower Re (Re=50) compare to the Re=200 in both MBSR and TMAC scheme. As the accommodation coefficient increases to 0.1 the x-component velocity shows a small effect on slip for both MBSR and TMAC scheme followed by Fig. 4.12(a) and Fig. 4.12(c). The execution time

performing the computational simulation for the both schemes has been provided in Table 3. The information from Table 3 it is seen that TMAC scheme requires more time rather than MBSR scheme for both no-slip and slip boundary condition. Viewing the qualitative results, it may conclude that at the immediate layer near top wall MBSR provides 42.33 percentages more slip than TMAC.

Reynolds number (Re)	u-component velocity	v- component velocity
50	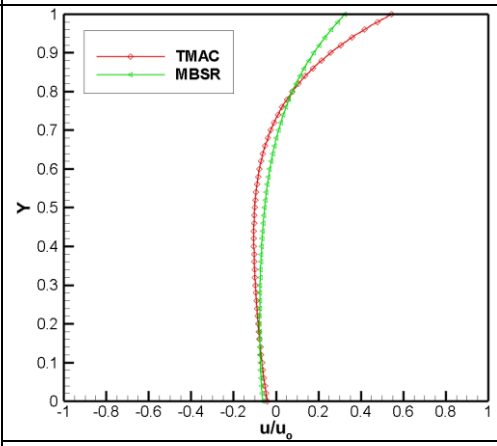	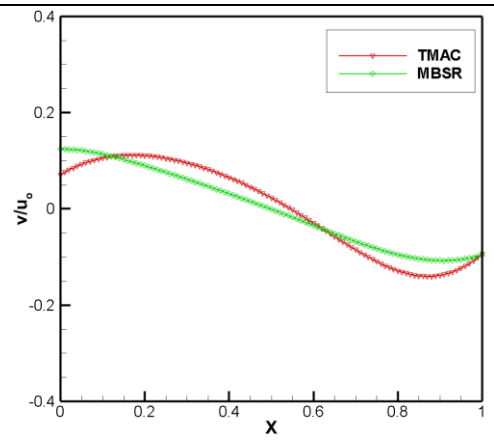
	(a)	(b)
200	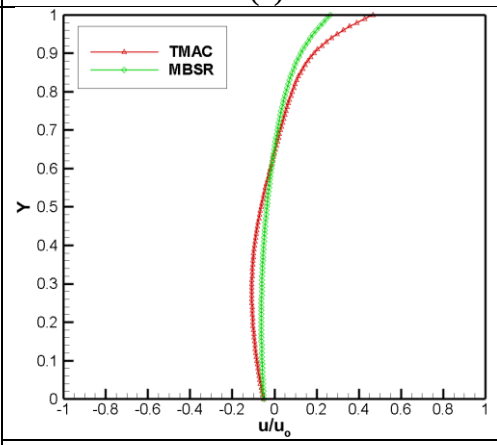	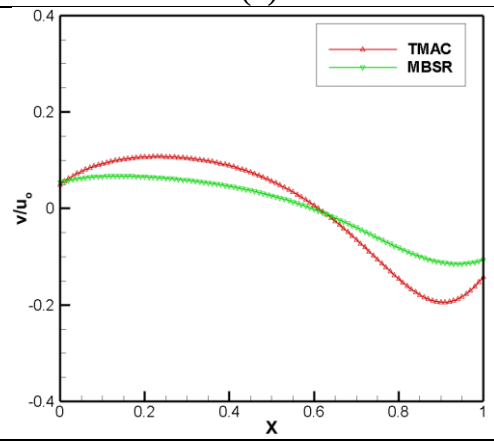
	(c)	(d)

Fig. 4.11 Comparison of TMAC and MBSR scheme through u and v plot at $\sigma = 0.01$: (a), (b) at Re=50 and (c), (d) at Re=200 respectively.

Reynolds number (Re)	u-component velocity	v- component velocity
50	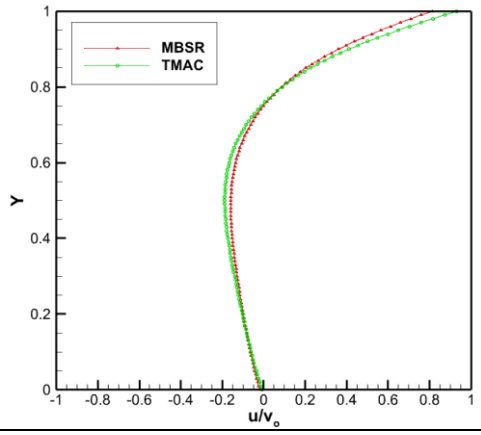	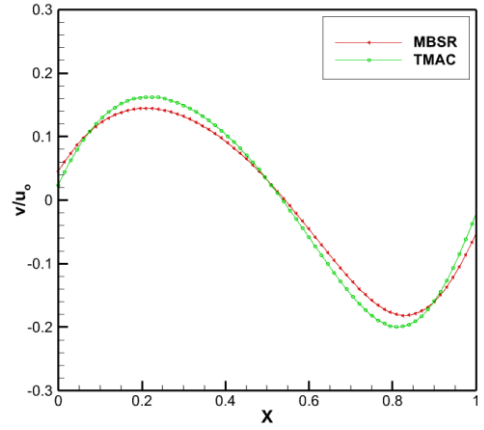
	(a)	(b)
200	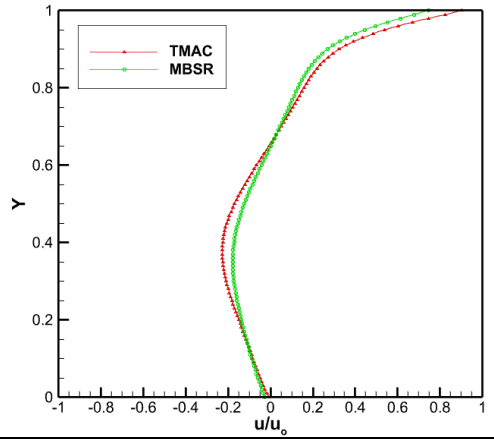	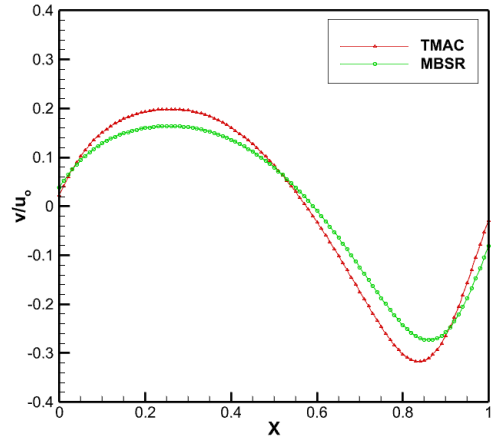
	(c)	(d)

Fig. 4.12 Comparison of TMAC and MBSR scheme through u and v plot at $\sigma = 0.1$: (a), (b) at Re=50 and (c), (d) at Re=200 respectively.

Figure 4.13 describes the streamline map at a particular Re (Re=50) with increasing σ values from maximum slip σ=0.01 to no-slip σ=1 condition towards the bottom. The left column of Fig. 4.13 corresponds to MBSR boundary scheme while the right column extends for TMAC boundary scheme. It is observed from the Fig. 4.13 (a) through Fig. (d) that, there is no secondary vortex generated in the right bottom corner of the cavity using both boundary scheme. Different flow characteristics have been observed in Fig. 4.13(e) and Fig. 4.13(f) for σ=0.1 in which no secondary vortex is formed in the cavity due to extra numerical slip generation for MBSR scheme (Fig. 4.13 (e)) while that secondary eddy near the right bottom corner of the cavity starts to form when TMAC is used according to Fig. 4.13(f). The supportive evidence on this flow behavior has been documented in Fig 4.12 (a) and (b). As the σ value increases towards no-slip condition secondary eddy grow in the close to the right bottom corner and the effect of slip reduces.

Accommodation coefficient (σ)	MBSR	TMAC
0.01	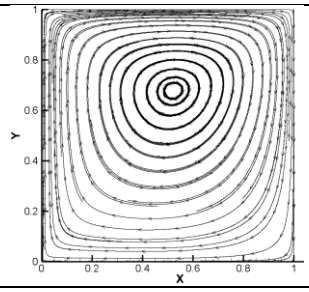	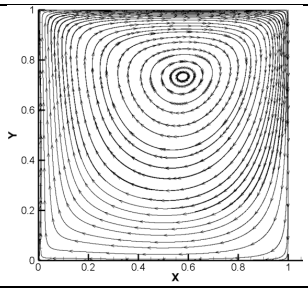
	(a)	(b)
0.05	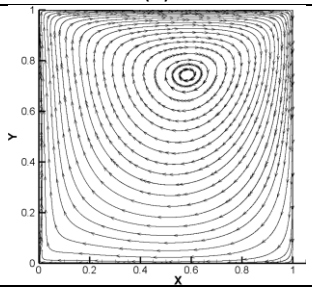	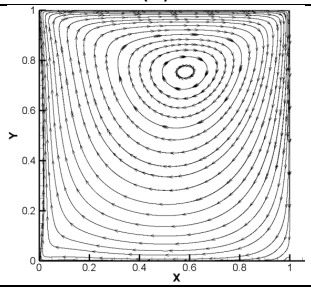
	(c)	(d)
0.1	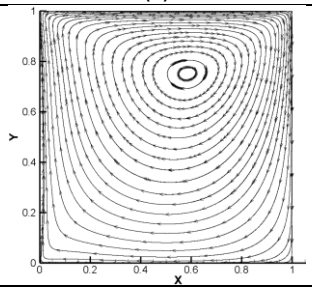	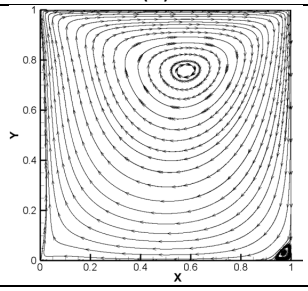
	(e)	(f)
0.5	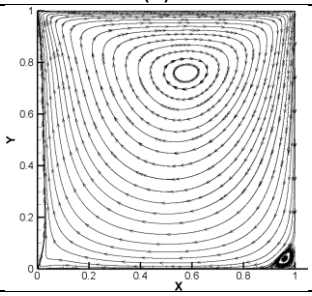	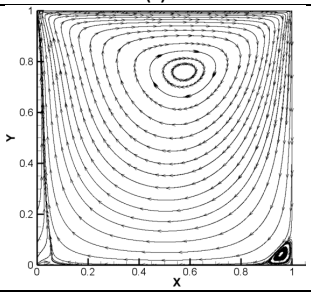
	(g)	(h)
1	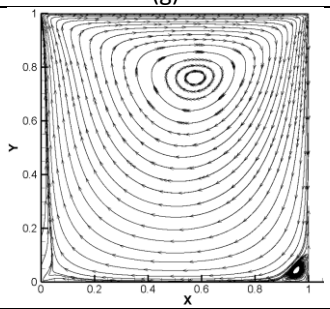	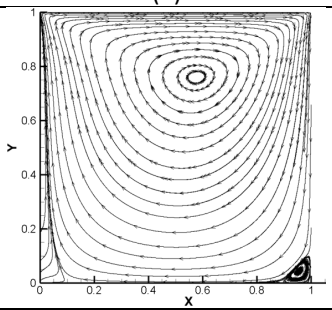
	(i)	(j)

Fig.4.13 Comparison in streamline plot of TMAC and MBSR at different accommodation coefficient at Re=50

4.5 Distribution of skin friction coefficient

The distribution of skin friction coefficient at different Re has been described at the bottom wall of the cavity in Fig. 4.14 for maximum slip and no-slip condition. A first order as well as second order analysis has been performed for both maximum and no-slip condition which is depicted in Fig. 4.14(a)-4.14(b) and 4.14(c)-4.14(d), respectively. It is observed from Fig. 4.14(a) and 4.14 (c) that with the increasing of Re skin friction coefficient is more at maximum slip due to the relative motion due to the velocity gradient between the bottom wall and its adjacent wall is more which incorporates more slippage to the fluid. Fig. 4.14(b) and 4.15(d) shows that at no slip condition (σ=1) the bottom wall does not show any slip effect due to the zero velocity at the bottom boundary. The left column of the Fig. 4.14 shows a comparison between 1st order (Fig. 4.14(a)) and 2nd order (Fig. 4.14(c)) skin friction coefficient at maximum slip condition. Results show that the second order skin friction coefficient gives better result than the first order. Similarly, comparison has been made for no slip condition which is describes in Fig. 4.14 (b) and Fig. 4.14(d). The first order and second order skin friction coefficient values are nearly same for no-slip boundary condition.

The first order and second order skin friction coefficient have been investigated at Re=20 and Re=300 incorporating maximum slip as well as no-slip boundary condition which is given in Fig. 4.15. It is seen from the Fig. 4.15(a) that at low Re (Re=20) the deviation between 1st order and 2nd order skin friction coefficient is less compare to higher Re value (Re=300) shown in Fig. 4.15(c) maintaining maximum slip. Fig. 4.15(b) and Fig. 4.15(d) implies the deviation of skin friction coefficient at no-slip condition from low Re to high Re respectively. The deviation of 1st order and 2nd order show similar nature to obtain skin friction coefficient values at no-slip boundary condition.

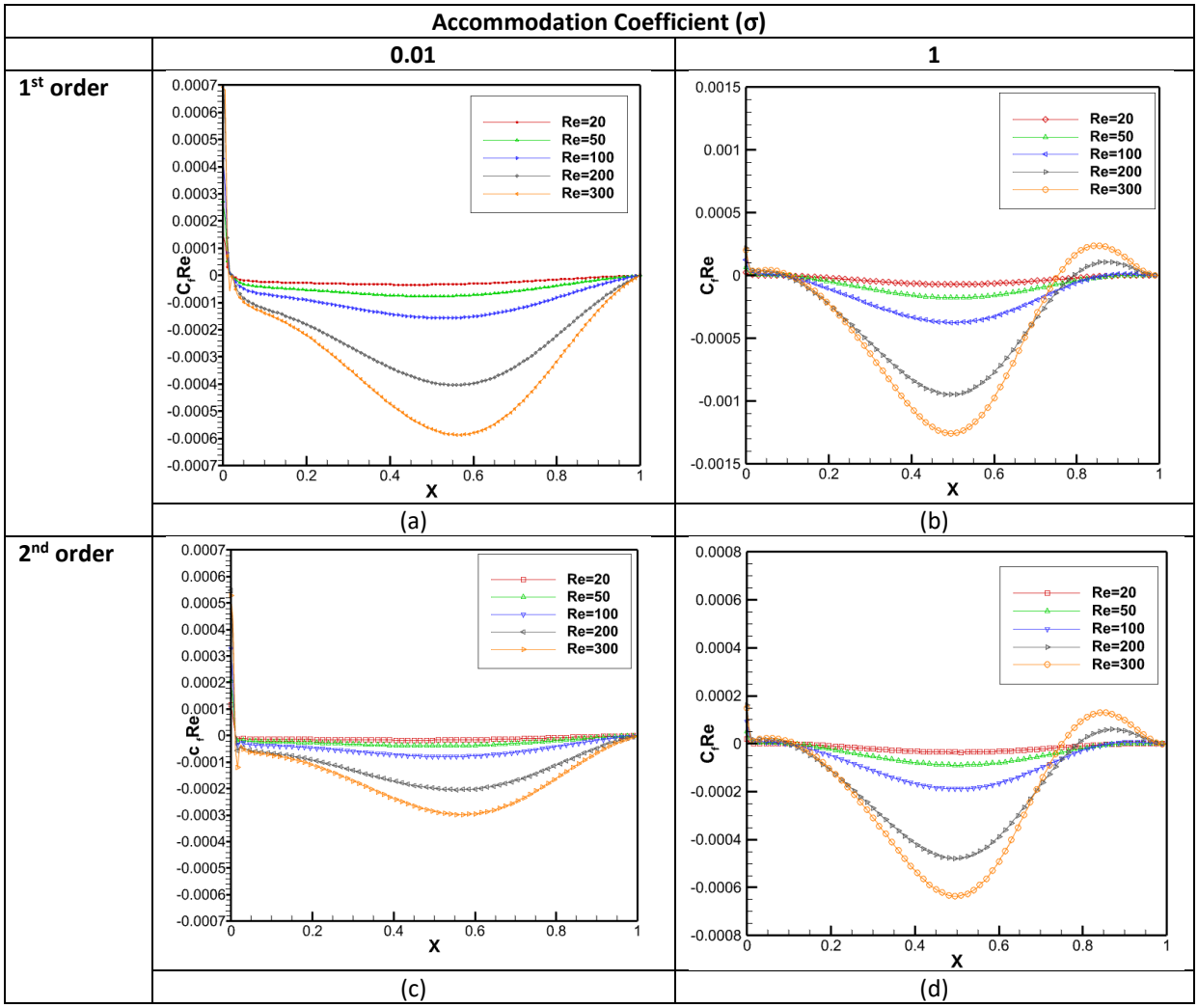

Fig.4.14 Distribution of Skin friction coefficient along south wall with maximum slip ($\sigma = 0.01$) and no-slip ($\sigma = 1$) condition at different Re number: (a) **1st order** (b) **2nd order**

Accommodation Coefficient (σ)		
Reynolds Number (Re)	**0.01**	**1**
20	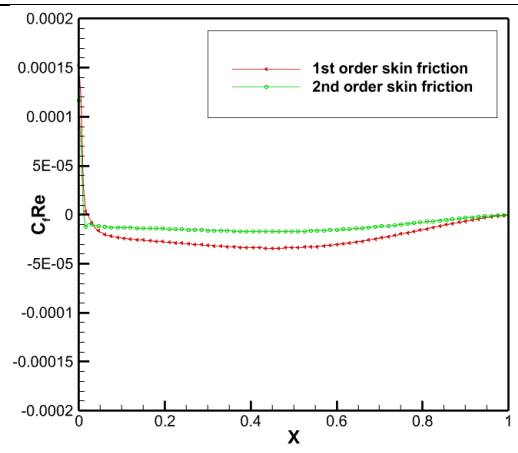	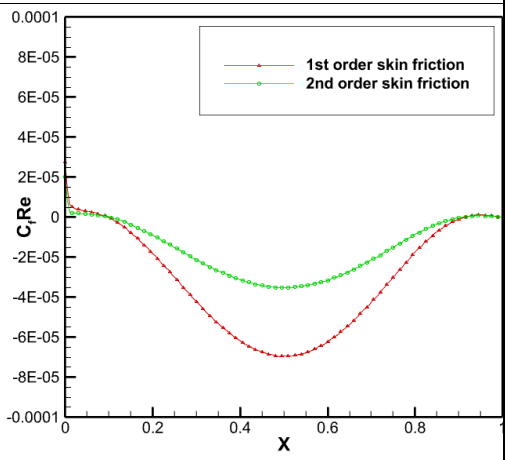
	(a)	(b)
300	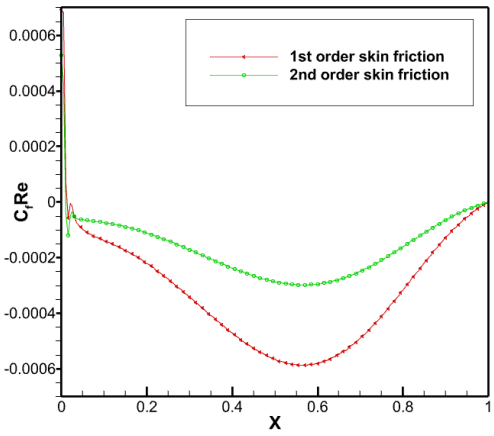	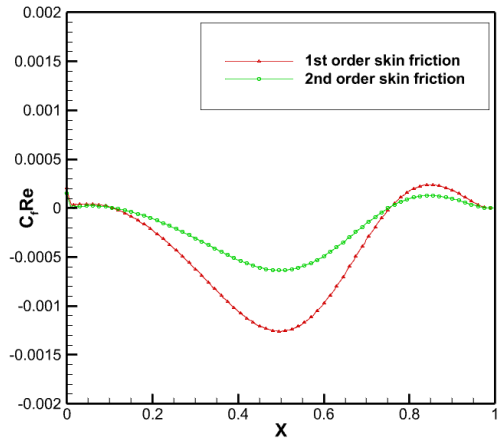
	(c)	(d)

Fig.4.15 Comparison of 1st and 2nd order skin friction with maximum slip ($\sigma = 0.01$) and no-slip ($\sigma = 1$) condition at different Re, (a) **Re=20** and (b) **Re=300**.

4.6 Comparison in execution time for TMAC and MBSR scheme

The execution time performing the computational simulation for the both schemes has been provided in Table II. The information from Table II it is seen that TMAC and MBSR both scheme take almost same time for both no-slip and slip boundary condition.

TABLE II. Comparison in execution time for TMAC and MBSR at Re=100 at different accommodation coefficient

Execution time (s) at different Accommodation coefficient (σ)					
Numerical Scheme	$\sigma = 0.01$	$\sigma = 0.05$	$\sigma = 0.1$	$\sigma = 0.5$	$\sigma = 1$
MBSR	1300.515	1299.029	1295.990	1297.682	1302.325
TMAC	1301.106	1303.080	1298.672	1300.630	1306.912

4.7 Location of primary and secondary vortex

The location of primary and secondary vortex has been provided for different slip coefficient (σ) at Reynolds number 20,50,100,200 and 300 in Table III. According to the information from Table III it is seen that location of primary vortex shifts towards the center of the cavity as slip increases. It is also seen that there is no trace of secondary vortex when maximum slip occurs at $\sigma = 0.01$. As the slip reduces that is σ increases, the secondary eddy near the right bottom corner of the cavity starts appearing onwards. From the tabulated data it is also clear that as the Reynolds number increases the size of the secondary eddy also increases.

TABLE III. Location of primary and secondary vortex at different Re number

Re	Accommodation Coefficient (σ)					
20	**Vortex Type**	0.01	0.05	0.1	0.5	1
	primary vortex	(0.53149, 0.73097)	(0.53652, 0.76053)	(0.53218, 0.76184)	(0.52973, 0.76285)	(0.53360, 0.76710)
	Secondary vortex	----------	----------	(0.97283, 0.02629)	(0.95766, 0.03309)	(0.95864, 0.03273)
50	primary vortex	(0.58102, 0.73310)	(0.58374, 0.75411)	(0.58488, 0.75622)	(0.59546, 0.77018)	(0.59552, 0.77331)
	Secondary vortex	----------	----------	(0.9699, 0.02936)	(0.95659, 0.04477)	(0.95043, 0.04475)
100	primary vortex	(0.62989, 0.71637)	(0.63206, 0.73559)	(0.62562, 0.73603)	(0.62886, 0.74261)	(0.62449, 0.74412)
	Secondary vortex	----------	(0.97926, 0.01868)	(0.95872, 0.04142)	(0.94352, 0.06192)	(0.94053, 0.06234)
200	primary vortex	(0.64635, 0.66159)	(0.62621, 0.66528)	(0.61593, 0.67221)	(0.61334, 0.68015)	(0.61363, 0.68464)
	Secondary vortex	----------	(0.95823, 0.04985)	(0.93272, 0.08258)	(0.91118, 0.10231)	(0.91046, 0.10587)
300	primary vortex	(0.63028, 0.60180)	(0.59672, 0.6191)	(0.58042, 0.62028)	(0.57753, 0.63157)	(0.57047, 0.63579)
	Secondary vortex	----------	(0.93772, 0.07628)	(0.91042, 0.09962)	(0.89642, 0.11683)	(0.89418, 0.12122)

Chapter 5

Conclusion

In this present work numerical simulation of liquid flow inside a square lid-driven cavity with slip boundary conditions has been presented using single relaxation time lattice Boltzmann method (SRT-LBM). In the slip regime SRT and MRT gives same results. The evidence of slippage near the walls and the effect of slip in the flow field has been presented in this project. The change in flow characteristics with different Reynolds number and Tangential momentum accommodation coefficient (TMAC) has been simulated in this work.

Two types of slip boundary conditions namely TMAC and MBSR has been used here. Both schemes moreover take same CPU time to execute the simulation but MBSR scheme provides more numerical slip than TMAC. The presence of secondary vortex near the right bottom corner of the cavity and growth of the secondary eddy gets affected significantly by slip coefficient (σ).

Comparing the simulation results with the results available in other literatures, it is found that the LBM simulation are in good agreement with the existing results.

References

[1] J. R. Koseff and R. L. Street, "The Lid-Driven Cavity Flow: A Synthesis of Qualitative and Quantitative Observations," *Journal of Fluids and Engineering*, pp.390-398, Dec 1984, doi: 10.1115/1.3243136.

[2] M. Morzynski and C. O. Popiel, "Laminar heat transfer in a two-dimensional cavity covered by a moving wall," *Numerical Heat Transfer*, vol. 13, no. 2, pp. 265–273, 1988, doi: 10.1080/10407788808910004.

[3] R. Iwatsu and J. M. Hyun, "Three-dimensional driven-cavity flows with a vertical temperature gradient," *International Journal of Heat and Mass Transfer*, vol. 38, pp.3319-3328, Dec. 1995, doi: 10.1016/0017-9310(95)00080-S.

[4] H. E. H. Meijer and C. P. J. M. Verbraak, "Modeling of Extrusion with Slip Boundary Conditions." *Polymer Engineering and Science,* vol. 28 no. 11, pp. 758-772, June 1988, doi: 10.1002/pen.760281108.

[5] J. M. Buick and J. A. Cosgrove, "Numerical simulation of the flow field in the mixing section of a screw extruder by the lattice Boltzmann model," *Chemical Engineering Science*, vol. 61, no. 10, pp. 3323–3326, May 2006, doi: 10.1016/j.ces.2005.11.070.

[6] M. A. Ismael, I. Pop, and A. J. Chamkha, "Mixed convection in a lid-driven square cavity with partial slip," *International Journal of Thermal Sciences*, vol. 82, no. 1, pp. 47–61, 2014, doi: 10.1016/j.ijthermalsci.2014.03.007.

[7] R. Samanta, H. Chattopadhyay, and C. Guha, "Transport phenomena in a differentially heated lid-driven cavity: A study using multi-relaxation-time thermal lattice Boltzmann modeling," *Physics of Fluids*, vol. 32, no. 9, Sep. 2020, doi: 10.1063/5.0021105.

[8] Y. Elguennouni, M. Hssikou, J. Baliti, and M. Alaoui, "Numerical study of gas microflow within a triangular lid-driven cavity," *Advances in Science, Technology and Engineering Systems*, vol. 5, no. 5, pp. 578–591, 2020, doi: 10.25046/AJ050571.

[9] D. V. Arumuga Perumal Gundaravarapu Kumar and A. K. Dass, "Application of Lattice Boltzmann Method to Fluid Flows in Microgeometries," *CFD Letters,* vol. 2 no. 2, June 2010.

[10] J. Baliti, M. Hssikou, and M. Alaoui, "Rarefaction and external force effects on gas microflow in a lid-driven cavity," *Heat Transfer - Asian Research*, vol. 48, no. 1, pp. 80–99, Jan. 2019, doi: 10.1002/htj.21369.

[11] B. John, X. J. Gu, and D. R. Emerson, "Investigation of heat and mass transfer in a lid-driven cavity under nonequilibrium flow conditions," *Numerical Heat Transfer, Part B: Fundamentals*, vol. 58, no. 5, pp. 287–303, Nov. 2010, doi: 10.1080/10407790.2010.528737.

[12] A. Mohammadzadeh, A. Rana, and H. Struchtrup, “DSMC and R13 modeling of the adiabatic surface,” *International Journal of Thermal Sciences*, vol. 101, pp. 9–23, Mar. 2016, doi: 10.1016/j.ijthermalsci.2015.10.007.

[13] A. Rana, M. Torrilhon, and H. Struchtrup, “A robust numerical method for the R13 equations of rarefied gas dynamics: Application to lid driven cavity,” *Journal of Computational Physics*, vol. 236, no. 1, pp. 169–186, Mar. 2013, doi: 10.1016/j.jcp.2012.11.023.

[14] Mizzi, S., D.R. Emerson, S.K. Stefanov, R.W. Barber and J.M. Reese, “Effects of rarefaction on cavity flow in the slip regime”, *Journal of Computational and Theoretical Nanoscience*, 2007. 4(4), p. 817-822.

[15] M. Darbandi, Y. Daghighi, S. Vakilipour, and G. E. Schneider, “Microflow in Lid-Driven Microcavity with Various Aspect Ratios,” *American Institute of Aeronautics and Astronautic*s, AIAA 2008-1285, June 2012, doi: 10.2514/6.2008-1285.

[16] A. Rana, M. Torrilhon, and H. Struchtrup, “A robust numerical method for the R13 equations of rarefied gas dynamics: Application to lid driven cavity,” *Journal of Computational Physics*, vol. 236, no. 1, pp. 169–186, Mar. 2013, doi: 10.1016/j.jcp.2012.11.023.

[17] E. B. Arkilic, M. A. Schmidt, and K. S. Breuer, “Gaseous Slip Flow in Long Microchannels,” *Journal of Microelectromechanical Systems*, vol. 6, no. 2, pp. 167-178, June 1997, doi: 10.1109/84.585795.

[18] X. He, Q. Zou, L.-S. Luo, and M. Dembo, “Analytic Solutions of Simple Flows and Analysis of Nonslip Boundary Conditions for the Lattice Boltzmann BGK Model.” *Journal of Statistical Physics* **87**, pp. 115-136, April 1997, doi: 10.1007/BF02181482.

[19] D. P. Ziegler, “Boundary Conditions for Lattice Boltzmann Simulations,” *Journal of Statistical Physics* **71**, pp. 1171-1177, June 1993, doi: 10.1007/BF01049965.

[20] C. K. Aidun and Y. Lu, “Lattice Boltzmann Simulation of Solid Particles Suspended in Fluid,” *Journal of Statistical Physics* **81**, pp. 49-61, Oct. 1997, doi: 10.1007/BF02179967.

[21] T. Inamuro, M. Yoshino, and F. Ogino, “A non-slip boundary condition for lattice Boltzmann simulations,” *Physics of Fluids*, vol. 7, no. 12, pp. 2928–2930, 1995, doi: 10.1063/1.868766.

[22] D. Hanel, “Lattice-Boltzmann simulation of gas-particle flow in filters,” *Computers and Fluids*, vol. 26, no. 7, pp. 697-712, Sep. 1997, doi: 10.1016/S0045-7930(97)00009-1.

[23] X. Shan, “Simulation of Rayleigh-Bé nard convection using a lattice Boltzmann method,” *Physical Review E - Statistical, Nonlinear, biological, and Soft Matter Physics*, vol. 55, no. 4, 2006, doi: 10.1103/PhysRevE.55.2780.

[24] M. Rohde, D. Kandhai, J. J. Derksen, and H. E. A. van den Akker, "Improved bounce-back methods for no-slip walls in lattice-Boltzmann schemes: Theory and simulations," *Physical Review E - Statistical Physics, Plasmas, Fluids, and Related Interdisciplinary Topics*, vol. 67, no. 6, p. 10, 2003, doi: 10.1103/PhysRevE.67.066703.

[25] S. Succi, "Mesoscopic Modeling of Slip Motion at Fluid-Solid Interfaces with Heterogeneous Catalysis," *Physical Review Letters*, vol.89, no. 6, 2002, doi: 10.1103/PhysRevLett.89.064502.

[26] Mohamed Gad-el-Hak, "The Fluid Mechanics of Microdevices-The Freeman Scholar Lecture," *journal of Fluids and Engineering*, vol. 121, no. 1, pp.5-33, March 1999, doi: 10.1115/1.2822013.

[27] X. Nie, G. D. Doolen, and S. Chen, "Lattice-Boltzmann Simulations of Fluid Flows in MEMS," *Journal of Statistical Physics* **107**, pp. 279-289, April 1997.

[28] M. Sbragaglia and S. Succi, "Analytical calculation of slip flow in lattice boltzmann models with kinetic boundary conditions," *Physics of Fluids*, vol. 17, no. 9, pp. 1–8, 2005, doi: 10.1063/1.2044829.

[29] V. Sofonea and R. F. Sekerka, "Boundary conditions for the upwind finite difference Lattice Boltzmann model: Evidence of slip velocity in micro-channel flow," *Journal of Computational Physics*, vol. 207, no. 2, pp. 639–659, Aug. 2005, doi: 10.1016/j.jcp.2005.02.003.

[30] Y. H. Zhang, X. J. Gu, R. W. Barber, and D. R. Emerson, "Capturing Knudsen layer phenomena using a lattice Boltzmann model," *Physical Review E - Statistical, Nonlinear, and Soft Matter Physics*, vol. 74, no. 4, 2006, doi: 10.1103/PhysRevE.74.046704.

[31] Z. Guo, T. S. Zhao, and Y. Shi, "Physical symmetry, spatial accuracy, and relaxation time of the lattice Boltzmann equation for microgas flows," *Journal of Applied Physics*, vol. 99, no. 7, Apr. 2006, doi: 10.1063/1.2185839.

[32] R. Benzi, L. Biferale, M. Sbragaglia, S. Succi, and F. Toschi, "Mesoscopic two-phase model for describing apparent slip in micro-channel flows," *Europhysics Letters*, vol. 74, no. 4, pp. 651–657, May 2006, doi: 10.1209/epl/i2006-10022-0.

[33] R. Benzi, L. Biferale, M. Sbragaglia, S. Succi, and F. Toschi, "Mesoscopic modelling of heterogeneous boundary conditions for microchannel flows," *Journal of Fluid Mechanics*, vol. 548, pp. 257–280, Feb. 2006, doi: 10.1017/S0022112005007512.

[34] Z. Guo, H. Han, B. Shi, and C. Zheng, "Theory of the lattice Boltzmann equation: Lattice Boltzmann model for axisymmetric flows," *Physical Review E - Statistical, Nonlinear, and Soft Matter Physics*, vol. 79, no. 4, Apr. 2009, doi: 10.1103/PhysRevE.79.046708.

[35] X. D. Niu, S. A. Hyodo, T. Munekata, and K. Suga, "Kinetic lattice Boltzmann method for microscale gas flows: Issues on boundary condition, relaxation time, and regularization," *Physical Review E - Statistical, Nonlinear, and Soft Matter Physics*, vol. 76, no. 3, Sep. 2007, doi: 10.1103/PhysRevE.76.036711.

[36] L. Zheng, Z. Guo, and B. Shi, “Microscale boundary conditions of the lattice Boltzmann equation method for simulating microtube flows,” *Physical Review E - Statistical, Nonlinear, and Soft Matter Physics*, vol. 86, no. 1, Jul. 2012, doi: 10.1103/PhysRevE.86.016712.

[37] L. Yang, Y. Yu, H. Pei, Y. Gao, and G. Hou, “Lattice Boltzmann simulations of liquid flows in microchannel with an improved slip boundary condition,” *Chemical Engineering Science*, vol. 202, pp. 105–117, Jul. 2019, doi: 10.1016/j.ces.2019.03.032.

[38] Z. Guo, C. Zheng, and B. Shi, “Lattice Boltzmann equation with multiple effective relaxation times for gaseous microscale flow,” *Physical Review E - Statistical, Nonlinear, and Soft Matter Physics*, vol. 77, no. 3, Mar. 2008, doi: 10.1103/PhysRevE.77.036707.

[39] Z. Guo, C. Zheng, and B. Shi, “Discrete lattice effects on the forcing term in the lattice Boltzmann method,” *Physical Review E - Statistical Physics, Plasmas, Fluids, and Related Interdisciplinary Topics*, vol. 65, no. 4, p. 6, 2002, doi: 10.1103/PhysRevE.65.046308.

[40] E. K. Ahangar, M. B. Ayani, and J. A. Esfahani, “Simulation of rarefied gas flow in a microchannel with backward facing step by two relaxation times using Lattice Boltzmann method – Slip and transient flow regimes,” *International Journal of Mechanical Sciences*, vol. 157–158, pp. 802–815, Jul. 2019, doi: 10.1016/j.ijmecsci.2019.05.025.

[41] Z. Guo, B. Shi, T. S. Zhao, and C. Zheng, “Discrete effects on boundary conditions for the lattice Boltzmann equation in simulating microscale gas flows,” *Physical Review E - Statistical, Nonlinear, and Soft Matter Physics*, vol. 76, no. 5, Nov. 2007, doi: 10.1103/PhysRevE.76.056704.

[42] W. A. Zahid, Y. Yin, and K. Q. Zhu, “Couette-Poiseuille flow of a gas in long microchannels,” *Microfluidics and Nanofluidics*, vol. 3, no. 1, pp. 55–64, Feb. 2007, doi: 10.1007/s10404-006-0108-5.

[43] L. S. Kuo and P. H. Chen, “A unified approach for nonslip and slip boundary conditions in the lattice Boltzmann method,” *Computers and Fluids*, vol. 38, no. 4, pp. 883–887, Apr. 2009, doi: 10.1016/j.compfluid.2008.09.008.

[44] K. Wang, Z. Chai, G. Hou, W. Chen, and S. Xu, “Slip boundary condition for lattice Boltzmann modeling of liquid flows,” *Computers and Fluids*, vol. 161, pp. 60–73, Jan. 2018, doi: 10.1016/j.compfluid.2017.11.009.

[45] Z. Guo, C. Zheng, and B. Shi, “Discrete lattice effects on the forcing term in the lattice Boltzmann method,” *Physical Review E - Statistical Physics, Plasmas, Fluids, and Related Interdisciplinary Topics*, vol. 65, no. 4, p. 6, 2002, doi: 10.1103/PhysRevE.65.046308.

[46] X. He and L.-S. Luo, “Theory of the lattice Boltzmann method: From the Boltzmann equation to the lattice Boltzmann equation,” *Physical Review E - Statistical, Nonlinear, biological, and Soft Matter Physics*, vol. 56, no. 6, pp. 6811-6817, 1997, doi: 10.1103/PhysRevE.56.6811.

[47] C. H. Marchi, R. Suero, and L. K. Araki, “The Lid-Driven Square Cavity Flow: Numerical Solution with a 1024 x 1024 Grid.” *Journal of the Brazilian Society of Mechanical Sciences and Engineering*, vol. 31, no. 3, Sept. 2009, doi: 10.1590/S1678-58782009000300004.

[48] L. Yang, Y. Yu, H. Pei, Y. Gao, and G. Hou, “Lattice Boltzmann simulations of liquid flows in microchannel with an improved slip boundary condition,” *Chemical Engineering Science*, vol. 202, pp. 105–117, Jul. 2019, doi: 10.1016/j.ces.2019.03.032.

[49] S. Mohammed and T. Reis, “Lattice Boltzmann method with moment-based boundary conditions for rarified flow in the slip regime,” *Physical Review E - Statistical, Nonlinear, biological, and Soft Matter Physics*, Oct. 2021, doi: 10.1103/PhysRevE.104.045309.